

SALVATORE MARTINO<sup>1</sup>, FRANCESCA BOZZANO<sup>1</sup>, PAOLO CAPOROSSO<sup>1</sup>,  
DANILO D'ANGIÒ<sup>1</sup>, MARTA DELLA SETA<sup>1</sup>, CARLO ESPOSITO<sup>1</sup>, ANDREA FANTINI<sup>2</sup>,  
MATTEO FIORUCCI<sup>1</sup>, LEONARDO MARIA GIANNINI<sup>1</sup>, ROBERTO IANNUCCI<sup>1</sup>,  
GIAN MARCO MARMONI<sup>1</sup>, PAOLO MAZZANTI<sup>1,3</sup>, CRISTINA MISSORI<sup>1</sup>,  
SERENA MORETTO<sup>1</sup>, STEFANO RIVELLINO<sup>1</sup>, ROBERTO WALTER ROMEO †<sup>4</sup>,  
PAOLO SARANDREA<sup>2</sup>, LUCA SCHILIRÒ<sup>1</sup>, FRANCESCO TROIANI<sup>1</sup>, CHIARA VARONE<sup>5</sup>

## GROUND EFFECTS TRIGGERED BY THE 24<sup>TH</sup> AUGUST 2016, M<sub>w</sub> 6.0 AMATRICE (ITALY) EARTHQUAKE: SURVEYS AND INVENTORYING TO UPDATE THE CEDIT CATALOGUE

**ABSTRACT:** MARTINO S., BOZZANO F., CAPOROSSO P., D'ANGIÒ D., DELLA SETA M., ESPOSITO C., FANTINI A., FIORUCCI M., GIANNINI L.M., IANNUCCI R., MARMONI G.M., MAZZANTI P., MISSORI C., MORETTO S., RIVELLINO S., WALTER ROMEO R.W., SARANDREA P., SCHILIRÒ L., TROIANI F. & VARONE C., *Ground effects triggered by the 24<sup>th</sup> August 2016, M<sub>w</sub> 6.0 Amatrice (Italy) earthquake: surveys and inventorying to update the CEDIT catalogue.* (IT ISSN 0391-9839, 2017).

The CEDIT catalogue, Italian acronym of Catalogue of Earthquake-Induced Ground Effects, is available since 2011. After the M<sub>w</sub> 6.0 Amatrice (Italy) earthquake (occurred at 01:36:32 UTC on 24<sup>th</sup> August, 2016) this catalogue was updated with 147 new inventoried ground effects. Since the first hours after the mainshock, field works and targeted remote sensing analyses were performed for recognizing and inventorying earthquake-induced ground effects. To avoid an inextricable overlap of ground effects due to either earthquake or rainfall events, intensive field activities were carried out and completed within a week, hence before the first intense rainfalls occurred on 30<sup>th</sup> of August. Ground effects mainly consist of landslides, in particular rock-falls and rock- and debris-slides, whereas less than 2% of the effects consist of ground cracks not directly related to landslides. The maximum distance from the

epicenter of the surveyed ground effects is about 36 km, though more than 50% of the effects occurred within 20 km. The plano-altimetric distribution of ground effects is rather conditioned by the presence of road cuts, as well as by local natural hillslope topographic and morphological setting. The 73% of the triggered landslides intercepted road-cuts and accounted for significant interference with local traffic and emergency activities. The altimetric distribution of the ground effects covers a range of about 1000 m (from 600 up to 1600 m a.s.l.), emphasising that the ground effects involved the outcropping rock masses in different topographic conditions. Moreover, the homogeneous distribution of the ground effects into the different outcropping lithological units suggests that lithology did not play a principal role as predisposing factor for the earthquake-induced slopes failures occurred in the area. This work presents the methodological approach used for efficiently recognizing and inventorying ground effects triggered by the 24<sup>th</sup> August 2016 (M<sub>w</sub> 6.0) Amatrice earthquake, as well as for managing and sharing results online on a global, pre-existing and public geo-database.

**KEY WORDS:** Earthquake-induced landslides, Inventory, CEDIT Catalogue, Rock slides, Rock falls, Apennines, Italy.

<sup>1</sup> Department of Earth Sciences and Research Center for the Geological Risks (CERI) of the Sapienza University of Rome, Italy.

<sup>2</sup> Tecnostudi Ambiente Srl., Rome, Italy

<sup>3</sup> NHAZCA S.r.l., spin-off Sapienza University of Rome, Rome (Italy)

<sup>4</sup> Department of Pure and Applied Sciences (DiSPeA), University of Urbino "Carlo Bo", Urbino (PU), Italy

<sup>5</sup> École Supérieure d'Ingénieurs des Travaux de la Construction (ESITC), 28 Avenue du Président Wilson, 94234, Cachan, France.

Corresponding author: S. MARTINO, salvatore.martino@uniroma1.it

This study was carried out in the framework of field work emergency activities, coordinated by the CERI research center of the Sapienza University of Rome. These activities were performed in co-operation with the University of Urbino "Carlo Bo", the Spin-off NHAZCA of "Sapienza" University of Rome and the company Tecnostudi Ambiente srl. The Authors wish to thank the forest rangers of the Corpo Regionale Guide Alpine Regione Marche and the National Park of the Mts. Sibillini for the logistic support provided.

Supplementary material related to this article can be found at: <https://gfdq.glaciologia.it/issues/>

**RIASSUNTO:** MARTINO S., BOZZANO F., CAPOROSSO P., D'ANGIÒ D., DELLA SETA M., ESPOSITO C., FANTINI A., FIORUCCI M., GIANNINI L.M., IANNUCCI R., MARMONI G.M., MAZZANTI P., MISSORI C., MORETTO S., RIVELLINO S., WALTER ROMEO R.W., SARANDREA P., SCHILIRÒ L., TROIANI F. & VARONE C., *Effetti deformativi al suolo indotti dal terremoto di Amatrice (Italia) M<sub>w</sub> 6.0 del 24 Agosto 2016: rilevamento e censimento per l'aggiornamento del catalogo CEDIT.* (IT ISSN 0391-9839, 2017).

Dal 2011 è disponibile per la consultazione, sul sito del Centro di Ricerca per i Rischi Geologici (CERI), il CEDIT (Catalogo italiano degli Effetti Deformativi del suolo Indotti dai forti Terremoti). A seguito del terremoto di Amatrice (Italia) di magnitudo M<sub>w</sub> 6.0 avvenuto alle 01:36:32 UTC del 24/08/2016, il CEDIT è stato aggiornato con 147 nuovi effetti sismoindotti censiti. A partire dalle prime ore dopo la scossa principale, rilevamenti di sito ed analisi mediante tecniche di telerilevamento sono state effettuate per l'identificazione ed il censimento degli effetti sismoindotti. Per evitare la sovrapposizione, difficilmente scindibile, tra effetti al suolo indotti dal terremoto e quelli causati da precipitazioni, un'attività di rilevamento intensivo è stata condotta e completata entro una settimana dal terremoto, prima degli intensi eventi di pioggia

avvenuti a partire dal 30 Agosto. Gli effetti sismoindotti più rappresentati tra quelli censiti consistono in frane, in particolare crolli, scorrimenti in roccia e flussi detritici, mentre meno del 2% degli effetti è costituito da fratture non direttamente relazionabili a frane. La massima distanza dall'epicentro degli effetti sismoindotti rilevati è pari a circa 36 km, benché più del 50% degli effetti sia stato rilevato entro i 20 km, mentre la loro distribuzione plano-altimetrica appare per lo più condizionata dalla presenza di tagli stradali, come anche da specifiche condizioni topografiche relazionabili all'assetto geomorfologico locale.

La distribuzione delle frane censite non rivela una correlazione con l'intensità macrosismica (MCS); ciò potrebbe essere spiegato considerando l'alta concentrazione degli effetti entro i primi 20 km dall'epicentro, dove è stata ottenuta un'ampia distribuzione delle classi di intensità macrosismica.

Il 73% delle frane innescate ha intercettato strade, causando una significativa interferenza con il traffico locale e le attività di emergenza. La distribuzione altimetrica degli effetti deformativi al suolo rilevati ricopre un intervallo di quote compreso tra i 600 e i 1600 m s.l.m. (ovvero circa 1000 m di dislivello), rimarcando che gli effetti deformativi al suolo sismoindotti hanno coinvolto affioramenti di ammassi rocciosi in differenti contesti topografici.

Inoltre, la distribuzione omogenea degli effetti sismoindotti in corrispondenza delle differenti unità litologiche affioranti, suggerisce che la litologia non abbia giocato un ruolo discriminante come fattore predisponente per le frane innescatesi nell'area. Per ciò che riguarda gli approcci metodologici sperimentati, l'analisi di immagini interferometriche satellitari (ottenute da Sentinel-1 e ALOS-2) e l'analisi di immagini ottiche, consistenti in ortofoto e foto aeree pre- e post-evento (Copernicus EMSR177), hanno reso possibile la visibilità di deformazioni gravitative a più grande scala non evolute in collasso (analisi interferometrica) e di eventi di frana localizzati nelle "zone rosse" (analisi ottica), interdette all'accesso per motivi di sicurezza.

Questo lavoro descrive l'approccio metodologico utilizzato sia per il rilevamento e la catalogazione degli effetti sismoindotti dal terremoto di Amatrice  $M_w$  6.0 del 24 Agosto 2016, che per la gestione e la condivisione in rete di una banca dati pubblica e a libero accesso.

La distribuzione degli effetti sismoindotti dal terremoto di Amatrice del 2016 appare complementare alle distribuzioni di effetti censiti a seguito dei precedenti forti terremoti dell'Umbria-Marche (1997) e de L'Aquila (2009) che hanno interessato aree limitrofe. Queste evidenze hanno colmato la lacuna storica sulla potenzialità di sismoinduzione legata a forti terremoti in Appennino centrale.

Si ritiene, inoltre, che la metodologia qui presentata possa essere estrapolata per il censimento degli effetti indotti dai successivi terremoti dell'Ottobre 2016 e del Gennaio 2017, che hanno interessato settori adiacenti dell'Appennino centrale.

**TERMINI CHIAVE:** *frane sismoindotte, censimento, catalogo CEDIT, scorrimenti in roccia, crolli, Appennino, Italia.*

## INTRODUCTION

Earthquake-induced landslides are generally responsible for severe damages and fatalities. Consequently, more than 50% of the total losses due to landslides in the World are to coseismic slope failures (Petley, 2012). Moreover, Bird & Bommer (2004) reported that the maximum damages caused by earthquakes are often related to landslide events. Several historical earthquake-induced landslides demonstrated the severity of such events, as they often involved areas, which have been intensely damaged by the seismic shaking. Among other examples, the latter was the case of Las Colinas landslide, which was triggered by the 13<sup>th</sup> January 2001 ( $M_w$  7.6) El Salvador earthquake and that caused about 585 fatalities (Evans & Bent, 2004). Earth-

quake-induced landslides can also trigger co-related phenomena, by a sort of "domino-effect", among which river damming and tsunamis as recently reported by Collins & Jibson (2015) for the 25<sup>th</sup> April 2015 Nepal earthquake.

Earthquake-induced landslides are also responsible for diffused and intense environmental changes, which often require high resilience by socio-economical systems to recover the *status quo ante* land-use conditions or modify them by readjustment or renovation strategies.

The most complete database of earthquake-induced ground effects in Italy (CEDIT) (Martino & alii, 2014 - <http://www.ceri.uniroma1.it/cn/gis.jsp>) is available online since 2011. The catalogue has the peculiarity to be constructed based on several historical documents covering a period of about one millennium, from 1000 AD to present days. The collected data demonstrate that landslides represent the most documented type of earthquake-induced ground failures, corresponding to almost 44% of the inventoried effects, which also include ground cracks, liquefaction and surface faulting.

Two different solutions could be jointed for advancing risk mitigation strategies concerning earthquake-induced landslides: i) inventorying the occurred earthquake-induced landslides, ii) providing a comprehensive hazard mapping, also for first-time earthquake-triggered slope failures. This jointed strategy takes advantage from past memories in order to outline the severity of occurred "domino-effect" scenarios driving toward future events. This is in agreement with a prevision approach for the risk management, which favours time-delayed and out-of-emergency solutions.

Keefer (1984) presented the expected distribution of earthquake-induced ground effects through a set of upper bound curves for the maximum distance of seismically induced landslides as a function of event magnitude, which was based on a dataset of 40 worldwide earthquakes. He grouped the types of landslides into three simple categories: disrupted slides and falls, coherent slides, and lateral spread and flows. For each group, he also proposed magnitude thresholds for earthquakes to induce landslides; the minimum magnitude of an earthquake that would cause disrupted landslides would be 4.0, with magnitudes 4.5 for coherent slides and 5.0 for flows and lateral spreads. Notwithstanding, he also indicated that landslides can be triggered by several causes, it would not be uncommon to find landslides induced by earthquakes of lower magnitudes when shaking occurred concurrently with other triggering factors, or when failure of the slope was imminent before the earthquake. In this sense, several examples of low magnitude induced landslides have been reported in the literature (Keefer, 1984; Rodríguez & alii, 1999; Papadopoulos & Plessa, 2000). In a recent review, Delgado & alii (2011) considered that the proposed upper bounds are appropriate in most cases, even if some outliers started to appear with each new dataset.

Several studies were concentrated on mapping inventory of coseismic landslides (Harp & Jibson, 1995; Meunier & alii, 2008; Gorum & alii, 2011; Xu & alii, 2014) revealing the distribution and density of landslides to be function of the distance from the seismogenic source, the earthquake

magnitude, and the fault properties (Keefer, 1984; Meunier & *alii*, 2007; Tatard & *alii*, 2010). Moreover, many studies, based on very rich and consolidated datasets (e.g. 1993  $M_w$  7.0 Papua New Guinea earthquake, the 1994  $M_w$  6.7 Northridge earthquake, the 2004  $M_w$  6.6 Niigata-Chuetsu earthquake, the 2008  $M_w$  7.9 Wenchuan earthquake, the 2008  $M_w$  6.9 Iwate-Miyagi Nairiku earthquake) accounted for the magnitude distribution of landslides, in terms of magnitude vs. frequency curves, that are largely used in seismic and non-seismic settings (Hovius & *alii*, 1997; Hungr & *alii*, 1999; Malamud & Turcotte, 1999; Stark & Hovius, 2001; Guzzetti & *alii*, 2002; Dussauge & *alii*, 2003; Stark & Guzzetti, 2009; Alfaro & *alii*, 2012a; Valagussa & Frattini, 2016). These studies underline that the frequency distribution exhibits power-law scaling for landslides larger than a size threshold but it also reveals a deflection below the modal peak of the distribution (“roll-over” effect by Malamud & *alii*, 2004) because of the incompleteness of the inventory (Guzzetti & *alii*, 2002). Nevertheless, several factors (Ashford & Sitar, 1997; Harp & Jibson, 2002; Bozzano & *alii*, 2011a; 2011b; Moore & *alii*, 2011; Lovati & *alii*, 2011; Alfaro & *alii*, 2012b) can condition the earthquake-induced landslide distribution among which topography, local seismic amplification and anthropic features (i.e. road cuts, man fills, previous intervention on slopes affected by landslide).

## THE 24<sup>th</sup> AUGUST 2016 EARTHQUAKE

After the 24<sup>th</sup> August 2016 ( $M_w$  6.0) Amatrice earthquake an extensive scenario of earthquake-induced ground effects appeared in the Central Apennines region struck by the earthquake shaking. As it resulted by the instrumental records (Lanzano & *alii*, 2016) the epicenter is located to the south of the municipality of Accumoli (Latitude 42.70° N, Longitude 13.23° E, depth 8.1 km) and the fault plane solution indicates normal faulting (strike 156°, dip 50°, rake -85°, length 26 km, width 16 km), which is in agreement with the regional tectonic style of the area, as well as with the complex structural setting including thrusts, blind normal faults, antithetic normal faults, which could be potentially reactivated in an extensional stress field (Boncio & *alii*, 2004a, 2004b; Meletti & *alii*, 2008; Bonini & *alii*, 2016).

The Italian Accelerometric Network (RAN) provided the records of the mainshock by 14 stations within 30 km and 42 within 50 km from the epicenter. The largest recorded PGVs are about 30 cm/s and 27 cm/s at two stations located in the Norcia intermontane basin. Values higher than 20 cm/s were also observed at the near-source stations of Amatrice (AMT- PGV = 21.5 cm/s) and at the farther station of Colfiorito, (CLF - PGV = 11.6 cm/s), both of them located 20 km far from the epicenter inside intermontane basins. The observed horizontal PGAs generally match the predictions according to the Sabetta & Pugliese (1987) attenuation law.

The seismic sequence spreads over a NNW-SSE trending, ~30 km long, ~15 km wide area. Interferometric Synthetic Aperture Radar (InSAR) elaborations based on various sensors and processing strategies (available at the

web-site [http://www.eorc.jaxa.jp/ALOS-2/en/img\\_up/dis\\_pal2\\_ita-eq\\_20160825.htm](http://www.eorc.jaxa.jp/ALOS-2/en/img_up/dis_pal2_ita-eq_20160825.htm)) depict a gently asymmetric, coseismic ground displacement pattern having two subsidence maxima of 15-20 cm east of Norcia and north of Amatrice. The first post-earthquake field surveys (EMERGE-GEO, 2016) revealed an alignment of surface breaks (fissures, open fractures and centimeter cracks). As it regards the macroseismic field (Galli & *alii*, 2016a), the most severe effects are focused south of the instrumental epicenter, in the Amatrice intermontane basin, where intensity ( $I_{MAX}$ ) reached 10-11 MCS; the epicentral intensity ( $I_0$ ) is 10 MCS. According to the DBMI 2015 database (available at the web-site <http://emidius.mi.ingv.it/CPTI15-DBMI15/>), the Amatrice area felt several historical strong earthquakes since the first half of the 17<sup>th</sup> century. On 7<sup>th</sup> October 1639 a first event ( $M_w$  6.2,  $I_0$  9-10 MCS) hit many villages close to Amatrice (9-10 MCS), causing severe damage in Amatrice itself (9 MCS) and Accumoli (8-9 MCS). On 28<sup>th</sup> April 1646, a second event hit once again some of the villages (9 MCS) causing severe damage also in Amatrice (8 MCS). The catastrophic 1703 and 1730 seismic sequences of Norcia and Valnerina caused once again a MCS 8-9 intensity in the Amatrice area. After these events and until the 24<sup>th</sup> August 2016 the MCS intensity recorded at Amatrice was up to 7.

## GEOLOGICAL AND GEOMORPHOLOGICAL SETTING OF THE EARTHQUAKE AREA

The 24<sup>th</sup> August 2016 earthquake struck an area of about 2458 km<sup>2</sup> in the Central Apennines encompassing the Marche, Latium and Umbria administrative regions, delimited to the SE by the Mt. Gorzano ridge, to the NE by the Mt. Vettore ridge, to the SW by the Mt. Giano Massif and, finally, to the S by the Reatini Mts. The area also includes the Cascia, Norcia, Castelluccio, Amatrice, Campotosto, and Montereale intermontane basins (fig. 1a). Minor effects were inventoried westward of the Reatini Mts. and in the southern sectors of the area (i.e. Gran Sasso Massif). The considered area is characterised by a structural setting that is the result of a multi-phase tectono-stratigraphic evolution (e.g. Cantalamessa & *alii*, 1982; Bally & *alii*, 1986; Ghisetti & Vezzani, 1991; Calamita & *alii*, 2003; Bigi & *alii*, 2011) including: i) the uplift of the imbricate fold-and-thrust architecture of the Apennine chain from the Miocene to the lower Pliocene, which involved a meso-cenozoic stratigraphic succession of limestone, marl and turbidites; ii) the normal faulting that, starting from Late Pliocene-Early Pleistocene, originated the Amatrice basin, SW of the Mt. Gorzano ridge, as well as the intermontane basins, SW of Mt. Vettore.

The sedimentary sequence outcropping in this sector includes Jurassic-Cenozoic deposits referred to the pelagic (Umbria-Marche basin) and carbonate platform (Latium-Abruzzi platform) domains (Ciarapica & Passeri, 2002; Pierantoni & *alii*, 2013), and the eastward migration of the Apennines chain caused the formation of eastward younger foreland basin systems (Ricci Lucchi, 1986; Argnani & Ricci Lucchi, 2001). The foreland basin formed in the area struck

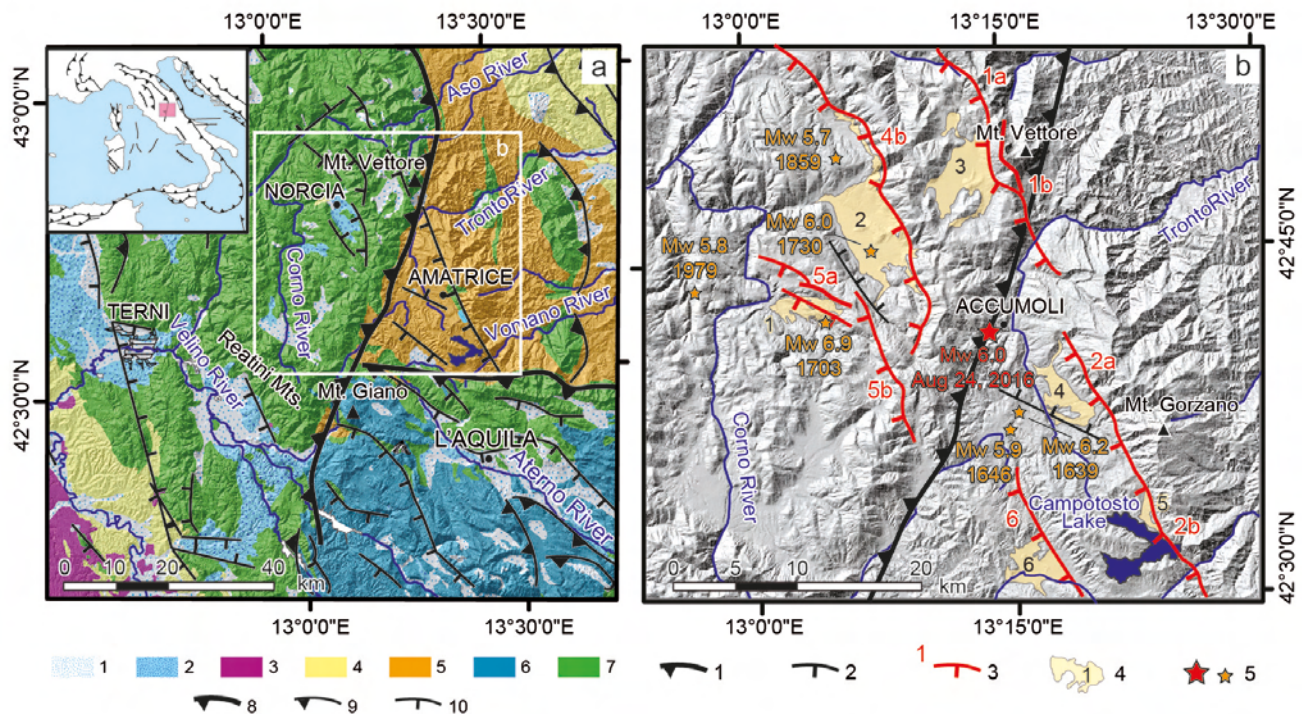


FIG. 1 - a) Simplified geological map of the study area; 1 continental Pleistocene-Holocene deposits; 2 continental Villafranchian deposits; 3 Pleistocene volcanic products; 4 Plio-Pleistocene marine sediments; 5 Tortonian-Messinian terrigenous deposits; 6 Triassic-Miocene Latium-Abruzzo platform limestones and dolomites; 7 Triassic-Miocene Umbria-Marche pelagic limestones and marls; 8 major thrust front; 9 thrust fault; 10 normal fault. b) 24<sup>th</sup> August 2016 ( $M_w$  6.0) earthquake epicentral area; 1 major thrust front; 2 normal fault; 3 active normal fault (1a: Mt. Bove fault, 1b: Mt. Vettore fault, 2a: Mt. Gorzano fault, 2b: Campotosto fault, 4b: Notoria-Mt. Pizzuto fault, 5a: Cascia fault, 5b: Castel S.Maria-Cittareale fault, 6: Montereale fault); 4 intermontane basin (1: Cascia Plain, 2: Norcia Plain, 3: Castelluccio Plain, 4: Amatrice Plain, 5: Campotosto Plain, 6: Montereale Plain); 5: earthquake epicenters.

by the Amatrice earthquake is filled by Cenozoic terrigenous turbiditic deposits (e.g. Laga fm., Upper Miocene; Falcini & alii, 2009) and evaporite formations (e.g. Gessoso-solfifera fm.). During Middle Pliocene-Early Pleistocene, the inner axial part of the Apennines chain emerged as a continental domain, while in the eastern sector, i.e. the Periadriatic basin, the marine environment persisted (Centamore & Nisio, 2003), leading to the deposition of thick pelitic successions. Several intermontane depressions, originated by the extensional tectonics progressively migrating eastward (Bigi & alii, 1997; Nisio, 1997), were filled by Quaternary lacustrine, landslide and alluvial deposits.

Concerning the structural setting, the NNE-SSW striking Olevano-Antrdoco regional paleo-structure (Cipollari & Cosentino, 1991) was reactivated as the lateral ramp of the Sibillini thrust front, which emplaced the Umbria-Marche domain onto the Lazio-Abruzzi domain (Bigi & Costa Pisani, 2005; Pace & alii, 2015). Several active extensional fault segments (fig. 1b) can be observed in the hanging wall and footwall of the outermost sector of the Olevano-Antrdoco-Sibillini Mts. sheet. They pertain to the Central Apennines Fault System (CAFS), which is a multi-scalar seismogenic fault structure including strike-slip and normal/transensional active fault segments (Tondi & Cello, 2003; Boncio & alii, 2004a). Among them, the NNW-SSE

striking Mt. Vettore normal fault is about 18 km long and formed a major intermontane basin, i.e. the Castelluccio Plain. The NW-SE-trending Mt. Gorzano-Campotosto normal fault is 30 km long, bounding two intermontane basins (i.e. the Amatrice and Campotosto plains), which are located along the northern and southern portions of the fault, respectively (Cacciuni & alii, 1995).

The activity of these systems during Holocene has been testified also by different geomorphological and paleoseismological studies (Pizzi & Galadini, 2009 and references therein). However, while historical surface faulting occurred along the Norcia-Mt. Fema segment during the 1703 earthquake and possibly during the 1979 earthquake (fig. 1b), the Mt. Vettore-Mt. Bove fault system seems to have been silent in historical times, since the latest surface faulting event is not more recent than the 6<sup>th</sup>-7<sup>th</sup> century AD (Galadini & Galli, 2003).

The long-term landscape evolution of this sector of the Apennines has been controlled, with progressively decreasing importance, by regional uplift, normal faulting and climate oscillations over the Quaternary. Uplift and normal faulting have caused the deactivation of this ancient landscape (testified by relict remnants according to Demangeot, 1965) through the entrenchment of the Tronto River drainage network that underwent frequent and strong re-organi-

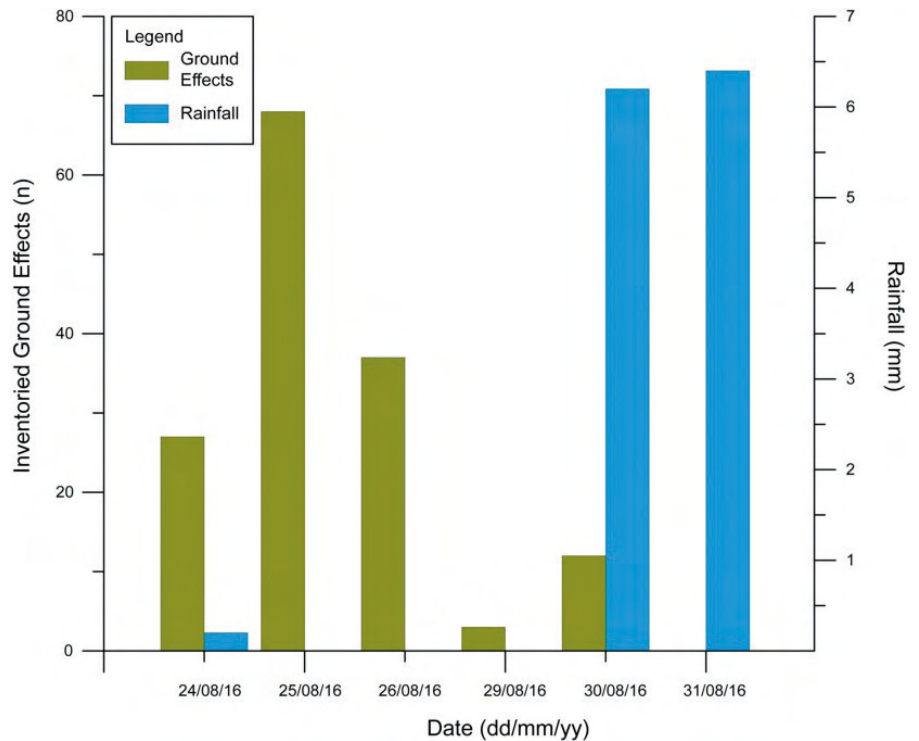


FIG. 2 - Time schedule of field works, with the number of ground effects inventoried for day and the cumulative daily rainfall.

zation phases, as already testified for other sectors of central Apennines (Aringoli & *alii*, 2014; Fubelli & *alii*, 2014). Geomorphic evidence of drainage flow inversions and lateral thinning of the continental deposits testify to the presence of also smaller basins originally closed and then captured by headward eroding rivers, as a consequence of normal faulting that cut also the continental deposits (Cacciuni & *alii*, 1995).

The structural control on the morphogenesis is also amplified by the outcrop of contrasting lithological units with high dip angles. Therefore, selective erosion favoured the formation of narrow and deep valleys alternated to linear ridges, on top of which some historical villages have been built. Such morphostructures, along with the high spatial variability of lithological units, concurred to the site effects of the 24<sup>th</sup> August 2016 Amatrice earthquake.

## EARTHQUAKE-INDUCED GROUND EFFECTS

### *Field evidence and geo-localisation of the records*

The field surveys devoted to inventorying the ground effects triggered by the 24<sup>th</sup> August ( $M_w$  6.0) earthquake were carried out within a 50-km large buffer centered on the epicentral area and they were intensively performed for one week after the seismic event, to avoid the superposition of effects caused by the first intense rainfall event, up to 6.5 mm cumulate in one day, started on 30<sup>th</sup> August (fig. 2).

The field surveys allowed inventorying 147 earthquake-induced ground effects (see the dataset reported in the supplementary material): 145 landslides and 2 ground

cracks. Based on morphological evidence, the landslides were classified for type of mechanism, according to Varner (1978): 128 rock falls, 10 rock slides and 7 debris slides were recognised (fig. 3a, 3b, 3c, 3d).

The adopted surveying criteria were focused on distinguishing the most recent landslides respect to the older ones, as well as to provide a high reliability of the earthquake trigger interpretation. In this regard, specific field evidence were considered for the different landslide mechanisms.

In case of rock falls and rock slides the following were considered:

- a clearly visible source area: clean and white surfaces, not weathered or vegetated scarps;
- a clearly visible rock mass debris: clean debris, not weathered or vegetated blocks, blocks over vegetation;
- a clearly visible track of rolled blocks;
- a detectable impact point of blocks.

In case of debris slides the following evidences were considered:

- remobilized debris: chaotic deposit overlapping the older accumulation surface;
- evidence of perimeter ground cracks (due to the detachment of debris above the bedrock);
- evidence of open ground cracks within debris with fresh vegetation cover.

In case of reactivation of translational or roto-translational landslides the following evidences were collected:

- ground cracks cutting paths, roads or soil and involving fresh vegetation;
- debris accumulation at the landslide toe over roads or paths.

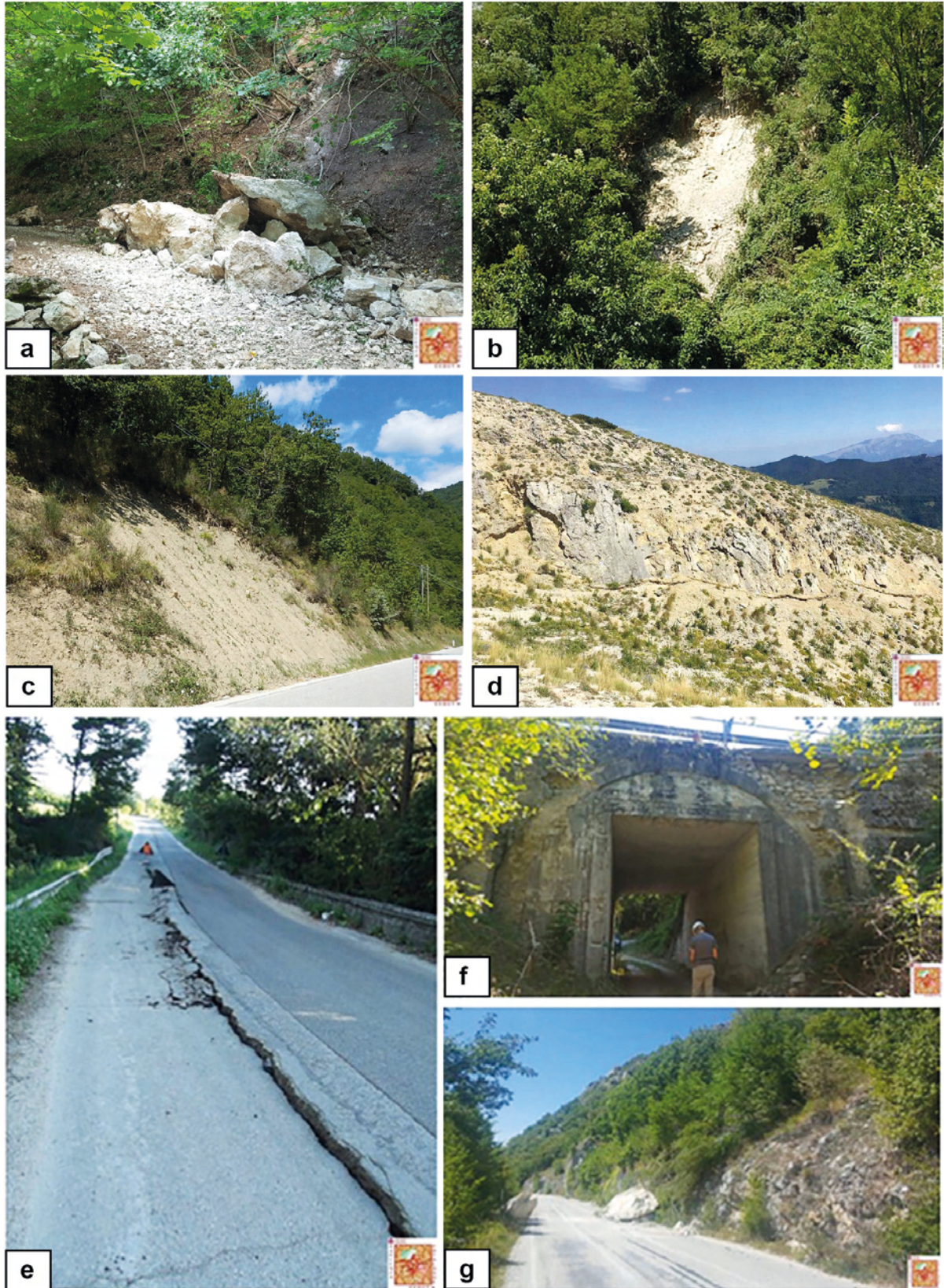


FIG. 3 - Examples of inventoried ground effects: rock fall (a); rock slide (b); debris slide (c); ground crack (d). Examples of ground effects interacting with infrastructures and lifelines: ground crack due to a landslide observed along a roadway (e); structural damages of a bridge (f); rock block on a roadway (g).

During the field activities, each ground effect was localised by Global Positioning System (GPS) also by the use of open source and user-friendly applications for mobile devices. For the induced ground effects near to roads or pathways, a GPS waypoint directly on new geomorphological features was marked. For the ground effects observed farther than 50 m from roads or paths, the GPS coordinates were fixed by considering the azimuthal direction and distance (measured by laser rangefinder) between the point of view (of the surveyor) and the source area to locate it on satellite images (Google Earth) and checking the location reliability.

The collected evidence of earthquake triggered landslides, was compared with the national landslide inventory (IFFI Project, ISPRA - <http://www.progettoiffi.isprambiente.it/cartanetiffi/>), and checked by the most recent satellites (Google Earth imagery; between years 1984 and 2016, depending on the availability in the area of interest), in order to exclude effects already existing before the earthquake.

The volume of each inventoried landslide was estimated by attributing one of the following volume classes (fig. 4a):

- class A: volume lower than 1 m<sup>3</sup>; 50 landslides were assigned to this class;
- class B: volume between 1 m<sup>3</sup> and 5 m<sup>3</sup>; 74 landslides were assigned to this class;
- class C: volume larger than 5 m<sup>3</sup>; 11 landslides were assigned to this class.

Only for 10 landslides it was not possible to attribute a reliable class because of the reduced visibility of the debris. Based on the above reported data, 50% of the inventoried landslides can be referred to class A, 34% to class B and the remnant 8% to class C.

Moreover, the following three categories of ground effects were distinguished based on the interaction with roads, pathways and infrastructures (e.g. bridges, roads) (figs. 4b, 3e, 3f, 3g; see also the thematic maps reported in the supplementary material):

- interferent: for ground effects that involve infrastructures; 105 ground effects were assigned to this category;
- not interferent: for ground effects that do not involve infrastructures; 26 ground effects were assigned to this category;
- possible interference: for the ground effects capable to involve infrastructures for secondary mobilization; 13 ground effects were assigned to this category.

As it regards the administrative distribution of the inventoried effects, 27% occurred in the Arquata del Tronto municipality, 22% in the Norcia municipality, 20% in the Accumoli municipality and 12% in the Amatrice municipality. Other 17 municipalities were involved in the earthquake-triggered effects. For the Arquata del Tronto and Amatrice municipalities, the density reached 0.5 inventoried ground effects over 1 km<sup>2</sup>. The cumulative estimated volume is of almost 100,000 m<sup>3</sup>, mostly occurring within 20 km from the earthquake epicenter.

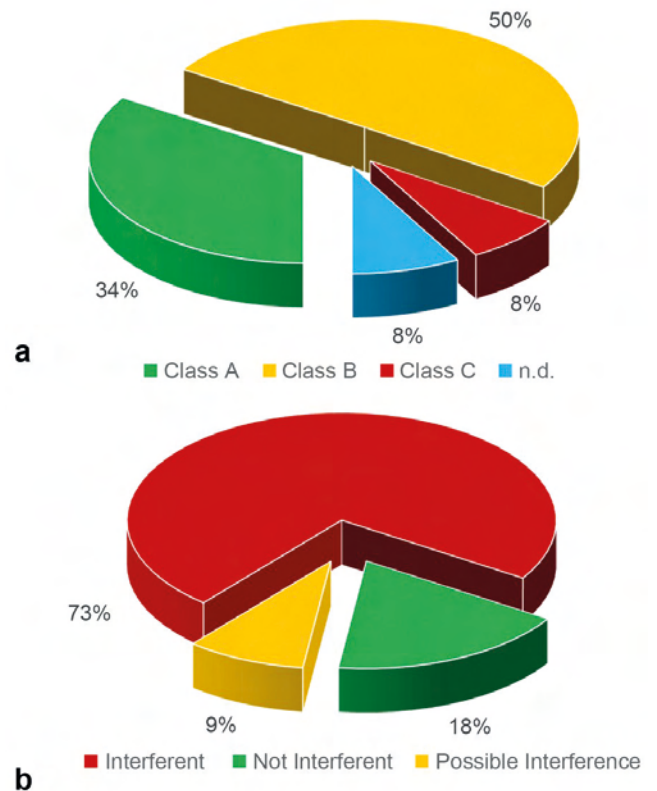


FIG. 4 - a) Percentage distribution of volume classes of the ground effects inventoried. b) Percentage distribution of interaction between the ground effects and the main infrastructures.

#### *Interferometric and optical analysis by satellite remote sensing*

Some slope deformations triggered by the 24<sup>th</sup> August 2016 ( $M_w$  6.0) Amatrice earthquake were detected by the satellite D-InSAR (Differential Synthetic Aperture Radar Interferometry) technique, which uses SAR images at different time to obtain interferometric differential maps. Such an interferogram implies the same acquisition geometry and the resulting output summarises different contribution expressed in the form:

$$\phi_{\text{int}} = \phi_{\text{flat}} + \phi_{\text{topo}} + \phi_{\text{disp}} + \phi_{\text{atmo}} + \phi_{\text{err}}$$

where  $\phi_{\text{flat}}$  is the flat earth phase,  $\phi_{\text{topo}}$  is the topography phase,  $\phi_{\text{disp}}$  is the displacement phase,  $\phi_{\text{atmo}}$  is the phase related to different atmospheric conditions and  $\phi_{\text{err}}$  represents the error related to uncontrolled effects (e.g. decorrelation, position along the satellite orbit). By subtracting the contributions due to  $\phi_{\text{topo}}$ , by the use of a Digital Elevation Model (DEM), as well as to  $\phi_{\text{flat}}$ , by the use of specific algorithms, it is possible to obtain the contribution at the interferogram due to  $\phi_{\text{disp}}$ . Nevertheless, in the so derived interferogram both the  $\phi_{\text{atmo}}$  and the residual height contribution (related to the difference between the topography and the DEM) still remain, which can be estimated through an advanced (A-DInSAR) processing.

We used SAR images available from Sentinel-1A, Sentinel-1B and ALOS-2 satellites. The Shuttle Radar Topog-

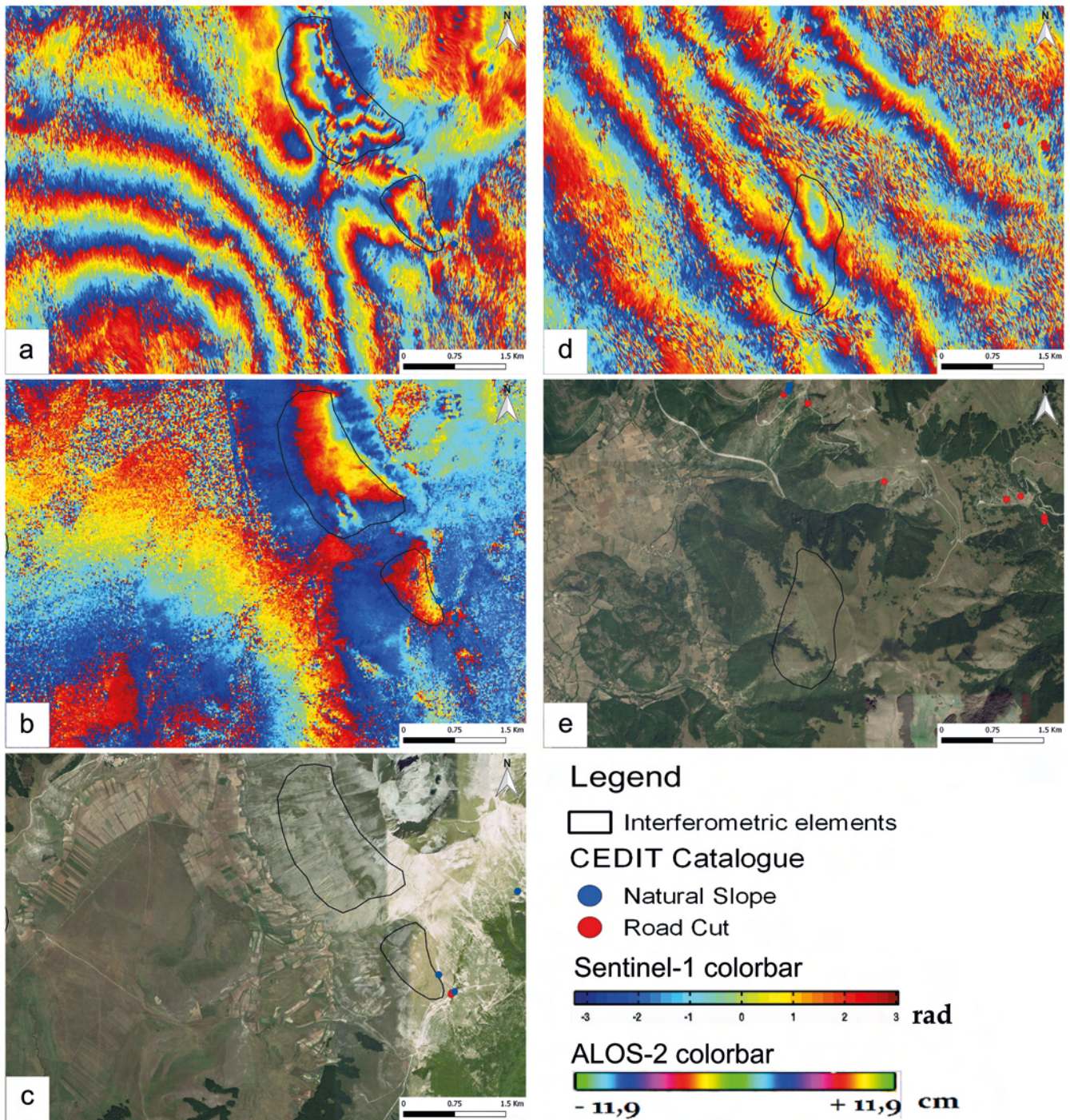


FIG. 5 - Ground effects inventoried by interferometric satellite images from Sentinel-1 (a) and ALOS-2 (b) images. Polygons 1 and 2 enveloping the deformation effects are compared with the field inventoried ground effects (c). Ground effects inventoried by interferometric satellite images from Sentinel-1 (d) images. The polygon 3 enveloping the deformation effects are compared with the field inventoried ground effects (e).

raphy Mission DEM (SRTM DEM) at a ground resolution of 30 m was used for subtracting the topography phase.

The interferograms from Sentinel-1A and 1B satellites were obtained by the software SARPROZ (SAR PROCESSING tool by periZ) while the interferograms for the ALOS-2

satellite images were available by the JAXA Earth Observation Research Center (EORC) (at the web-site - <http://www.eorc.jaxa.jp>).

For the analyses here presented, 3 interferograms by Sentinel-1 satellite (1 for the descending and 2 for the

ascending geometry) and 2 interferograms by ALOS-2 satellite (1 for the descending and 1 for the ascending geometry) were used. The Sentinel-1 images, captured in TOPSTAR acquisition mode, have a resolution of 5 x 20 m in the range and azimuth direction respectively. The interferograms ALOS-2 were obtained from images, captured in Stripmap mode, have a resolution of 10 m.

The Sentinel-1 images are characterised by a wavelength ( $\lambda$ ) of 5.6 cm (C Band) while ALOS-2 by a  $\lambda$  of 23.6 cm (L Band); therefore, the Sentinel-1 images allowed a higher resolution to be reached in terms of deformation mapping.

By comparing the interferograms obtained from the different wavelength images it was possible to point out deformation evidence on slopes to be related with earthquake-triggered effects. These elements are characterised by fringes having a higher gradient respect to adjacent zones. Figure 5 shows three examples of polygons where interferometric evidence of displacement are present; two of them (polygons 1 and 2) were identified on both the Sentinel-1 and ALOS-2 interferograms (figs. 5a, 5b) while the third one (polygon 3) is evident in the higher-resolution Sentinel-1 interferogram only, by the C Band (fig. 5d).

The interferometric evidence represent wide slope deformations characterised by centimeter-scale displacements along hillslopes. Polygons 1 and 2 are located on the Mt. Vettore (i.e. high-mountain area) (fig. 5c), while polygon 3 is located in the Forca Canapine area (fig. 5e). This last polygon does not correspond to specific ground effects surveyed in the field and inventoried in the CEDIT, since the resolution of the interferometric images is not suitable to distinguish the class A of rock falls detected in the field. On the contrary, polygons 1 and 2 correspond to ground cracks already surveyed in the field activities by direct observations (fig. 5).

To perform a more complete detection by remote sensing of the earthquake-triggered ground effects, optical satellite images available on the official web-site “Copernicus – Emergency Management Service” (<http://emergency.copernicus.eu/mapping/list-of-components/EMSR177>) were

also used. In this case, a more traditional aerial-photo interpretation led to a change detection optical analysis.

As an example, the results obtained in the case of Pescara del Tronto area are here discussed by comparing the field observations and the aerial photo-interpretation. In particular, a couple of images from the following Copernicus EMSR177 thematic maps were considered:

- pre-earthquake orthophotos, taken on 2014 by the Consorzio TeA (e-GEOS S.p.A., CGR S.p.A and Aerodata Italia Srl formats) with a spatial resolution of 50 and 20 cm/pixel;
- post-earthquake aerial photos, taken on 25<sup>th</sup> August 2016 by Aerial data © European Commission, with a spatial resolution of 10 cm/pixel.

In the Pescara del Tronto area, 10 landslides were inventoried by the photo-interpretation which include only 3 effects inventoried by field surveys (fig. 6). In this case, the aerial photos interpretation has been more effective with respect to the field surveying, even because the access to the village was prohibited or prevented due to either the collapsed buildings or the ongoing emergency actions.

## DATABASE AND INVENTORY

The surveyed ground effects were collected for updating the CEDIT database, already integrated with the effects related to the 2012 Emilia earthquake (Martino & *alii*, 2014). The database was organised into datasheets (Fortunato & *alii*, 2012). Each datasheet contains data about earthquakes and associated ground failures. The original relational database consists of tables at different levels of detail. A first table gathers seismological data, in chronological order, about events from which data concerning ground failures were obtained. Parameters describing the severity and location of the events are also given. The following catalogues were used: catalogues of earthquakes NT4.1.1 (Camassi & Stucchi, 1997) and CPTI04 (Gruppo di Lavoro CPTI, 2004), as well as catalogue of macroseismic effects DBMI04 (Stucchi & *alii*,

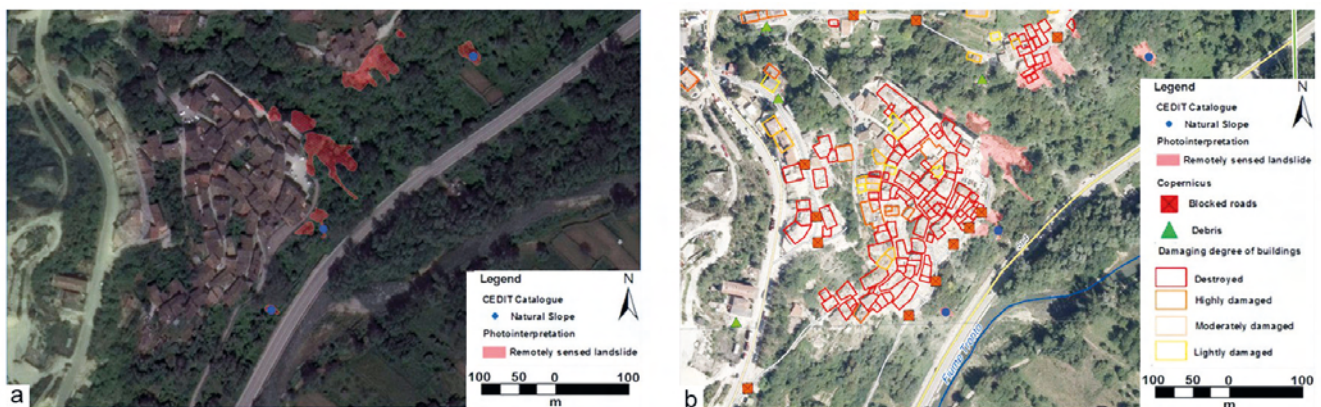


FIG. 6 - Examples of ground effects inventoried by aerial-photo interpretation from Copernicus EMSR177 thematic maps. Pre-earthquake (a) and post-earthquake (b) images were considered to perform a change-detection optical analysis.

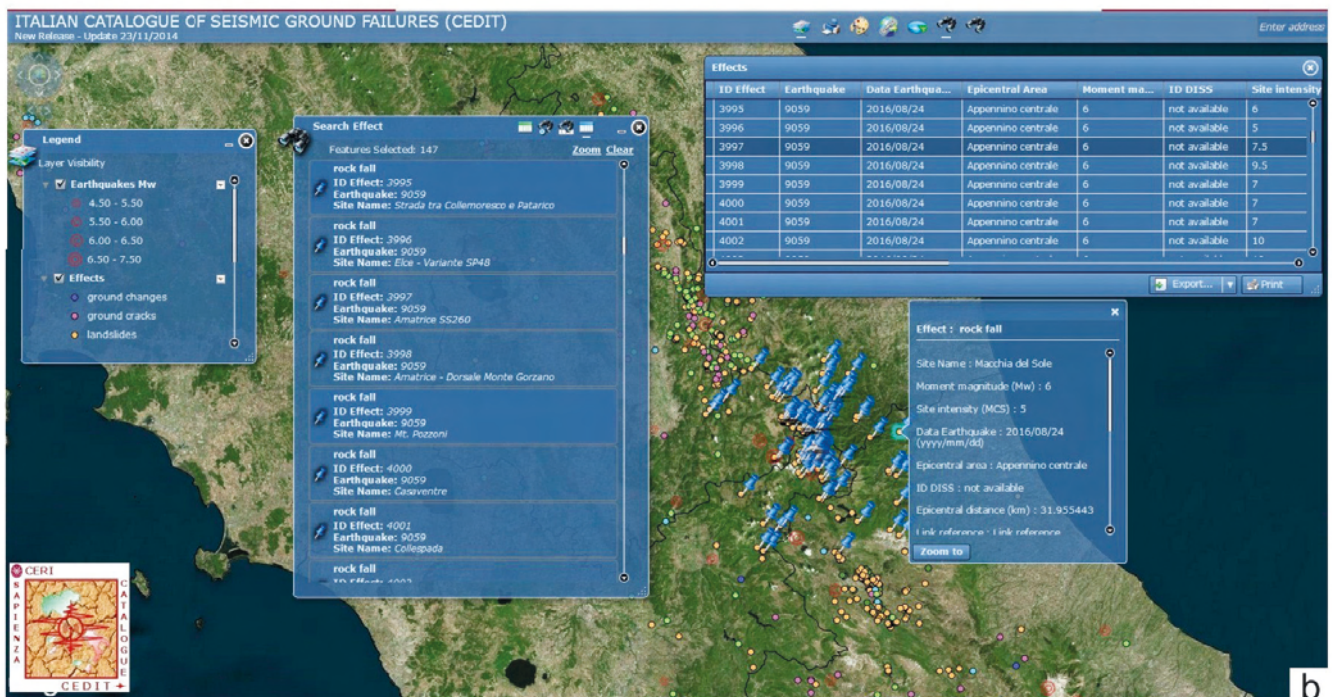
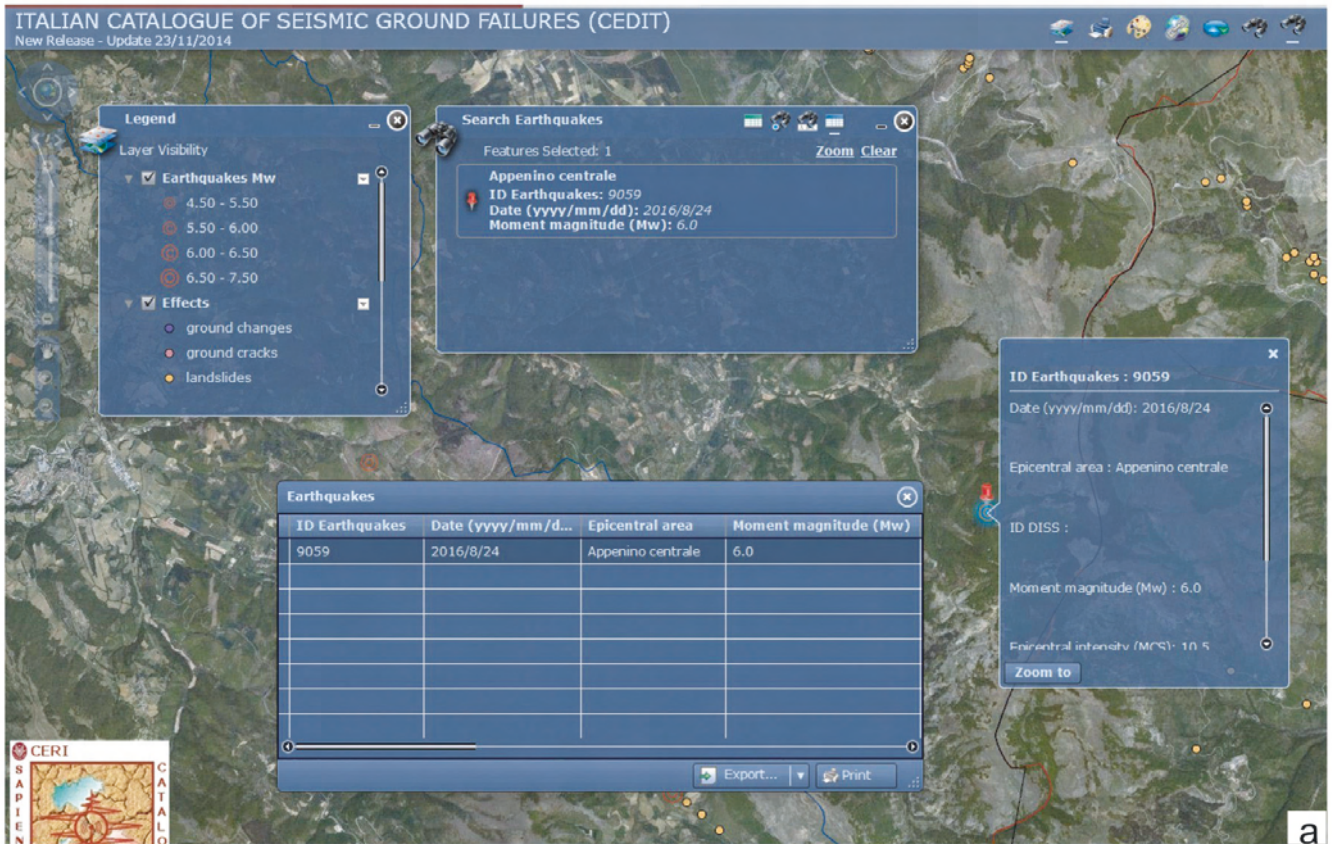


FIG. 7 - a) Example of CEDIT Web-GIS querying interface applied to the 24<sup>th</sup> August 2016 earthquake (the earthquake epicenter is shown by a red pointer). b) Example of CEDIT Web-GIS querying interface applied to the 24<sup>th</sup> August 2016 ground effects (blue pointers).

2007). With respect to the previous release of CEDIT, data were added about seismogenic sources retrieved from the DISS catalogue (INGV, 2010). A second table lists sites of ground failures associated with the seismic event. The sites are identified according to the ISTAT municipal code (available on the web-site <http://www.istat.it/it/>). A third table gives the quotations (e.g. original sentences), retrieved from historical sources, which describe the ground failures produced by the inventoried earthquakes. Each quotation refers to a single site and to one or multiple phenomena. To give a more detailed picture of the phenomenon, quotations by various authors about the same effect are also reported. The fourth table provides the details of the bibliographic sources used to search data about seismically-induced effects. Finally, a fifth table collects data on earthquake-induced ground failures obtained from the cited sources and includes macroseismic intensity assigned to the site (MCS), epicentral distance and involved lithology. Where available, also the intensity on the ESI scale (*Environmental Seismic Intensity scale*: Michetti & alii, 2004) is given.

In the CEDIT catalogue the ground failures are classified into five macrocategories in the following hierarchical order: landslides, ground cracks, liquefaction, surface faulting, ground level changes, each divided into subcategories which provide more details about phenomenological features (e.g. landslide mechanisms, punctual or linear liquefaction evidences).

## CEDIT ON-LINE CATALOGUE

The updated version of the CEDIT database is published online for public access at <http://www.ceri.uniroma1.it/index.php/web-gis/cedit/> and is hosted by the cloud web server of the Research Centre for the Geological Risks (CERI) of the Sapienza University of Rome.

The system was developed by using the services of ArcGIS® server based on ESRI™ technology. The system provides a geo-database consulting and querying interface with graph or table outputs (Martino & alii, 2014).

The CEDIT Web-GIS has an upper section including: menu for selecting layers and base maps; measuring editor; print options; search tool and Web-GIS link sharing key. The left section of the web-page includes an extensive legend of the different map layers selected from the TOP section. The earthquake layers and the regional boundaries are displayed at national scale. By increasing the level of detail, the user may also view the layers of the earthquakes-induced effects. Finally, the details section reports the metadata of the document and the references for its formal citation (Fortunato & alii, 2012).

Figure 7a shows an example of on-line querying of the CEDIT database. By clicking on the earthquake layer icon, the system will open a pop-up window with the following data:

- an upper list containing data about the site: CEDIT code identifying the seismic event; date of the event; area involved; macroseismic intensity MCS; magnitude  $M_w$ ;

The screenshot shows the CEDIT Web-GIS interface. At the top, a map shows the location of the site. The site information is as follows:

- Id effect:** 4018
- Site:** Villanova (Accumoli)
- Effects:** rock fall
- Lat:** 42.695 **Long:** 13.212

Below the site information is a table of references:

Sentence	ID reference	Title	Year	First author	Publishing
see the following picture	2452	Field surveys carried out by the CERI Working Group: S. Martino, P. Caporossi, M. Della Seta, C. Esposito, A. Fantini, M. Fiorucci, R. Iannucci, G.M. Marmoni, P. Mazzanti, S. Moretto, S. Rivellino, R.W. Romeo, P. Sarandrea, F. Troiani,	2016	S. Martino	on-line (CERI official Web-site)

Below the table is a photograph of the ground failure, showing a rock fall on a road. The photograph is titled "INTERFERENTE" and includes the following metadata:

- ID:** 38
- DATA\_RILE:** 25/08/2016
- LOCALITA:** Villanova
- TIPO\_FRANA:** Crollo in roccia
- DESCRIZION:** Crollo su taglio stradale
- LEGENDA:** INTERFERENTE
- LRN\_FOTO:** SMDGCH0608.jpg
- ID\_EFFETTO:** FR039
- FORTE:** CEDIT-2016
- QZ\_smpg:** 13.224587
- YZ\_mf:** 42.69082

At the bottom of the screenshot, there is a small text line: "ALIAN CATALOGUE OF EARTHQUAKE-INDUCED GROUND FAILURES (CEDIT) by FORTUNATO C., MARTINO S., PRESTININZI A. & ROMEO R.W. with the co-operation of FANTINI A. & SARANDREA P."

FIG. 8 - Example of CEDIT Web-GIS reference file referred to one of the ground effects triggered by the 24<sup>th</sup> August 2016 earthquake.

- a central list reporting the identification codes of the Parametric Catalogue of Italian Earthquakes – CPTI04 and of the Database of Individual Seismogenic Sources – DISS3.2.0, both with the related link to web-site of INGV (Istituto Nazionale di Geofisica e Vulcanologia, [www.ingv.it](http://www.ingv.it));
- a lower list giving the number of seismically induced effects by type.

Figure 7b shows an example of information that a user may view by clicking on the icon of the given type of effect; the example is referred to a rock fall inventoried during the last field surveys. The pop-up windows, which is opened by clicking on the icon present on the map, displays both data identifying the effect like code, site name, ISTAT site code, and data describing the associated earthquake like data, epicenter and local macroseismic intensity (where available). On the pop-up window, an upper-bound curve (magnitude vs. distance) for each ground effect is also reported, according to Keefer (1984). A link for downloading a \*.pdf file with the bibliographic sources available for the selected effect is also reported on the effect pop-up window (fig. 8). For ground effects surveyed after the 24<sup>th</sup> August 2016 earthquake, a picture of each inventoried effect was also included in the catalogue which is visible in the \*.pdf file with the bibliographic source.

After a validation procedure, the CEDIT database will be updated and implemented even considering the GEER and ISPRA official reports, as well as data from future scientific publications.

#### DISTRIBUTION OF EARTHQUAKE-TRIGGERED GROUND EFFECTS

Based on the inventoried landslides database, the most frequent typology is represented by rock fall (87%), followed by rock slide (6%) and debris slide (5%) (fig. 9a). The homogeneous distribution of effects over different lithological units reveals that lithology did not represent an exclusive predisposing factor to the landslides triggered by the 24<sup>th</sup> August 2016 earthquake. More in particular, pelagic limestone, marls and travertine were involved for the 43%, marly-arenaceous flysch for the 36% and limestone and dolomite for the 21% (fig. 9b).

According to the CEDIT database (Martino & *alii*, 2014) a macroseismic intensity (fig. 10) was attributed to each ground effect based on the macroseismic field (Galli & *alii*, 2016a, 2016b), i.e. considering the local macroseismic intensity (MCS) of the closest administrative locality. The distribution of landslides does not reveal a co-relation with MCS, that can be explained considering the high density of inventoried effect within 20 km from the epicenter, where a wide distribution of MCS intensity classes was obtained. A distribution analysis of total induced ground effects, including landslides and ground cracks have been carried out evaluating the frequency vs. epicentral distance defining a series of 1 km multi-ring buffers up to 50 km. Four zones corresponding to epicentral distances of 5 km, 10 km, 20 km and 50 km (labelled I, II, III and IV respectively), have been defined (fig. 11a).

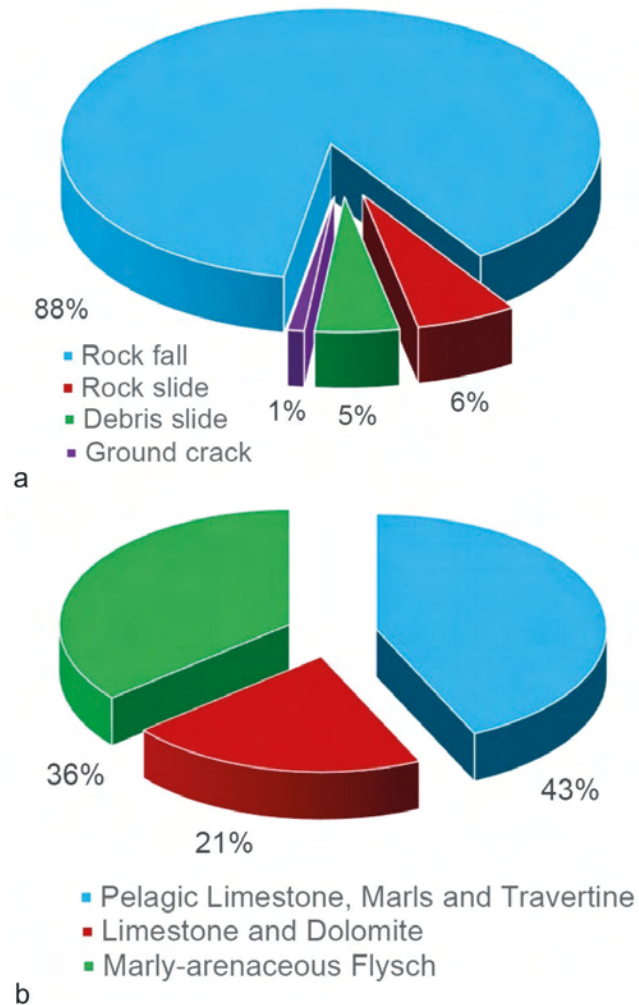


FIG. 9 - Percentage distribution of: a) landslide typology; b) involved lithological classes.

The distribution of epicentral distance *vs.* frequency of ground effects (fig. 11b) indicates that 49% of the inventoried effects occurred in zone I and II, 34% in zone III and the remnant 17% within zone IV.

Since the maximum epicentral distance observed for the earthquake-triggered landslides (namely “disrupted”, according to Keefer, 1984) is 36 km, this is coherent with the maximum expected distance of 80 km for  $M_w$  6.0, according to the global upper-bound curve by Keefer (1984), as well as with the maximum expected distance of 40 km for  $M_w$  6.0 according to the upper-bound curve from the CEDIT catalogue (instrumental age 1908-2012) by Martino & *alii* (2014).

Correlation of seismically induced effects with elevation indicates that 94% of events occurred in elevation range 600-1600 m a.s.l. (fig. 11c), with a maximum in the range 1000-1200 m a.s.l. (26% of effects). The 2.7% of the effects only is enclosed in the range 350-600 m a.s.l. At same time, the 3.3% of total ground effects occurred

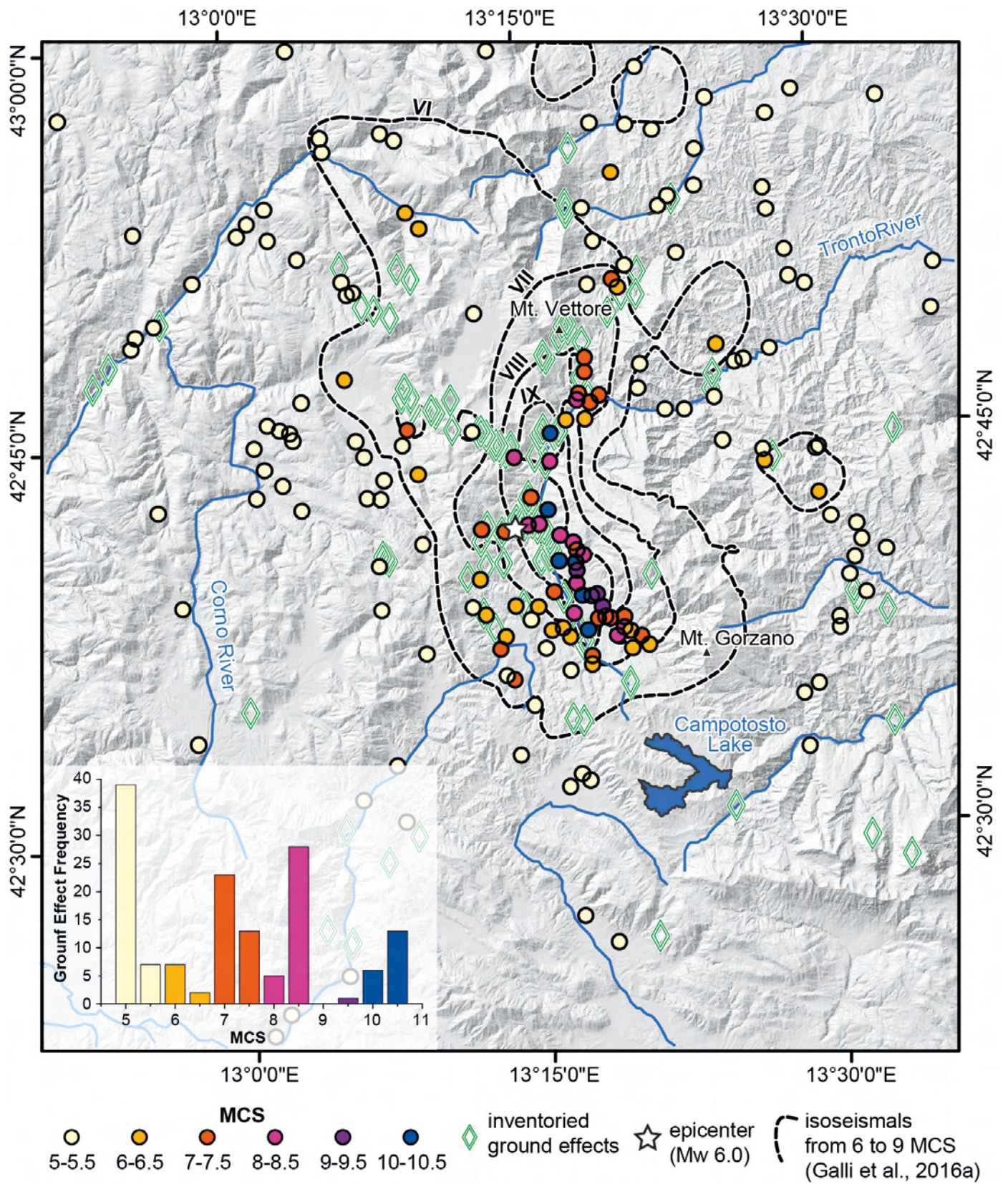


FIG. 10 - Macroseismic field from Galli & alii (2016a, 2016b) and distribution of ground effect frequency vs. MCS local intensity.

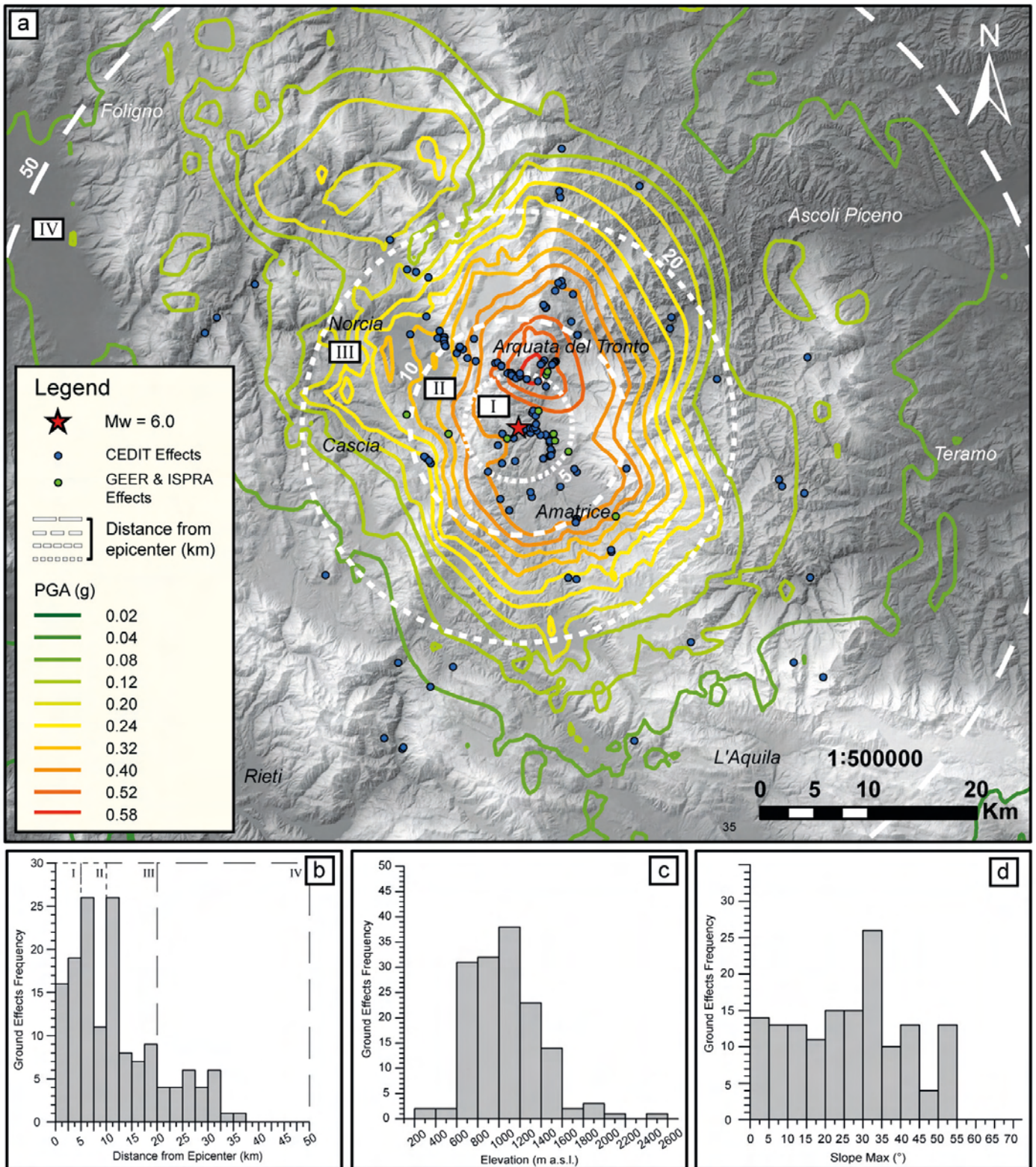


FIG. 11 - Distribution of triggered ground effects after the 24<sup>th</sup> August 2016  $M_w$  6.0 earthquake. a) shaking map (from INGV – <http://shakemap.rm.ingv.it/>) and inventoried ground effects (location of mainshock epicenter is also reported). Further ground effects reported by GEER and ISPRA working groups are also shown; b) earthquake-triggered ground effects distribution vs. epicentral distance; c) earthquake-triggered ground effects distribution vs. elevation; d) earthquake-triggered ground effects distribution vs. maximum slope (Zevenbergen & Thorne, 1987).

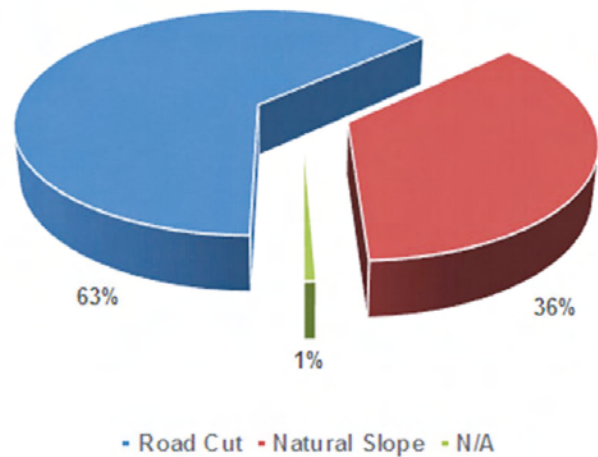
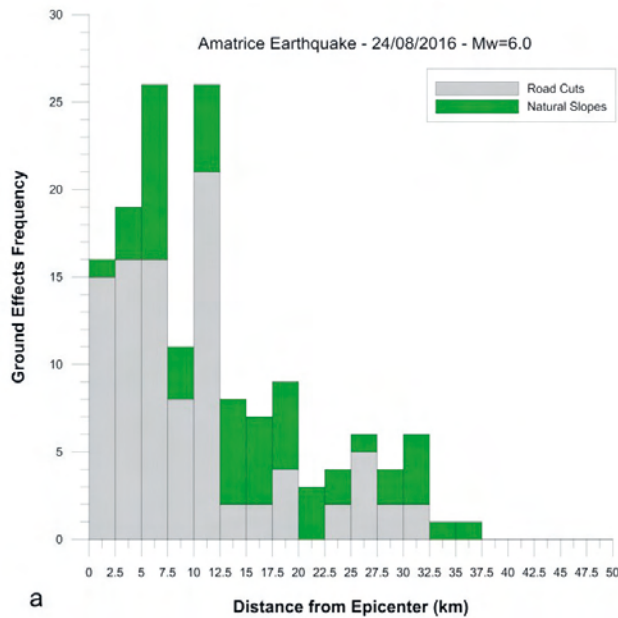


FIG. 12 - Distribution of ground effects triggered by the 24<sup>th</sup> August 2016  $M_w$  6.0 earthquake with epicentral distance (a) distinguishing occurrence on natural slopes and on man-made cuts (b).

at elevations higher than 1600 m a.s.l., where the highest slope values are observed.

The spatial correlation of landslides with maximum slope (Zevenbergen & Thorne, 1987) indicates that 45% of events occurred in the range 20°-40° degree (with a maximum of about 18% in the slope range 30°-35°) while only 20% of the events occurred on slope greater than 40° (fig. 11d).

Nevertheless, the not-null frequency of effects resulting for the lowermost slope classes (i.e. < 15°) outlines that the DEM resolution is not suitable for detecting topographic conditions related to the smallest class of landslide volume.

These results highlight a not direct control of slope on the landslides occurrence whereas steep slopes are less affected by seismically induced effects.

This finding seems not in good agreement with the results from Wartman & alii (2013) after their study on the  $M_w$  8.9 Tohoku earthquake in 2011 (Honshu, Japan) and Martha & alii (2017) after the Gorkha and Dolakha earthquakes (Nepal). In these studies, the most of the inventoried events are disrupted landslides (*sensu* Keefer, 1984) occurred at – or near – the crests of steep slopes.

Based on the above reported results is not possible to recognize a specific control factor on the landslide triggered by the 24<sup>th</sup> August 2016 earthquake; this is coherent with the homogeneous distribution of involved lithologies as well as with a not negligible effect due to man-made cut along roads or paths. Concerning this last feature, it is worth noting that 36% of the inventoried ground effects involved man-made cuts (fig. 12); this evidence explains some anomalous spatial clusters, such as in the case of the NW-SE alignment from Arquata del Tronto to Norcia (see fig. 11a) which just corresponds to a local road line.

By querying the CEDIT Web-GIS to compare the spa-

tial distribution of effects inventoried after the 24<sup>th</sup> August 2016  $M_w$  6.0 earthquake with the ones related to previous  $M_w$  6.0 1997 Umbria-Marche and  $M_w$  6.2 2009 L'Aquila earthquakes it is evident their complementarity respect to the adjacent seismogenic areas (fig. 13). Such an evidence fills the historical gap of the knowhow about such kind of earthquake-induced effects in Central Apennines.

The here reported statistical analysis is only referred to CEDIT catalogue; it does not include other reports (GEER Report, 2016; ISPRA Report, 2016), which represent 5% of entire statistical population. This assumption guarantees the homogeneity of the considered dataset, avoiding possible errors due to different survey techniques.

The here discussed methodology for surveying earthquake-induced ground effects was also experienced after the  $M_w$  5.9, 26<sup>th</sup> October, the  $M_w$  6.5, 30<sup>th</sup> October 2016 and the last  $M_w$  5.4, 18<sup>th</sup> January 2017 earthquakes, occurred in the same region of the Central Apennines. Hundreds of effects were already collected and inventoried in the on-line CEDIT catalogue (<http://www.ceri.uniroma1.it/index.php/web-gis/cedit/>). Based on such a huge dataset, further comparative analyses among the plano-altimetric distribution of all the earthquake-induced ground effects are going to be performed.

## CONCLUSIONS

The 24<sup>th</sup> August 2016,  $M_w$  6.0 earthquake that occurred in Central Apennines, caused 299 fatalities and heavy damages to several villages and towns, among which Accumoli, Amatrice, Arquata del Tronto and Pescara del Tronto. Field surveys spanning some days immediately

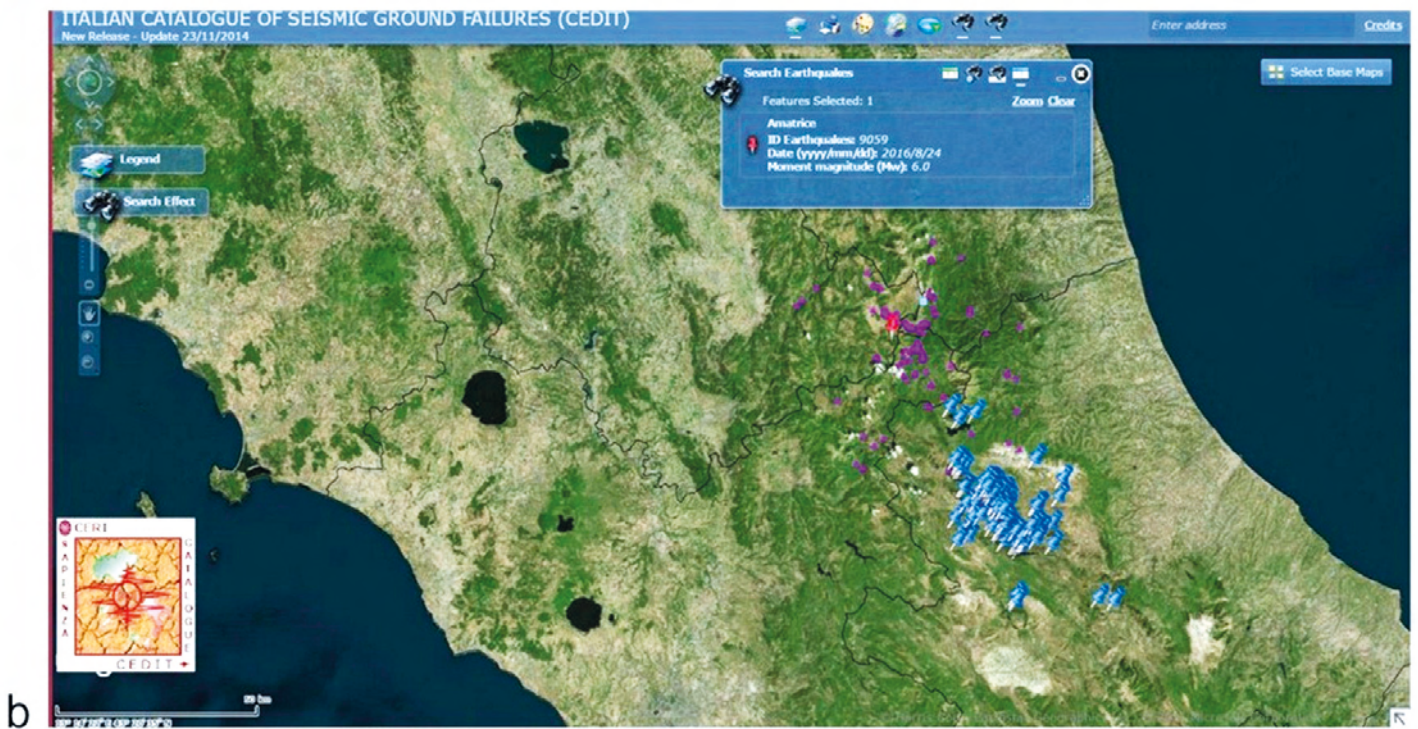
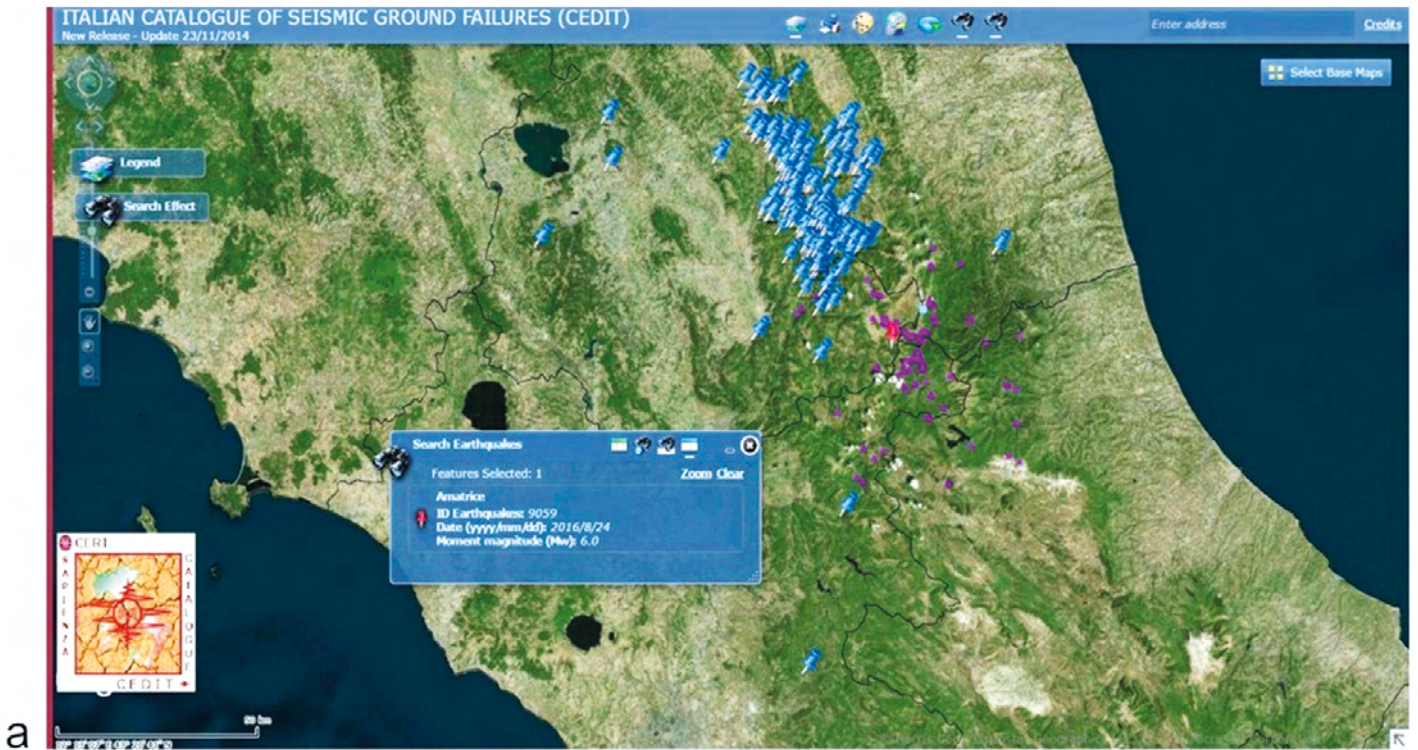


FIG. 13 - Distribution of ground effects triggered by the 24<sup>th</sup> August 2016  $M_w$  6.0 earthquake (pink colour) in comparison with the ones triggered by the 1997 Umbria-Marche (a) and 2009 L'Aquila (b) earthquakes plotted through the CEDIT Web-GIS masks. The epicenter of the 24<sup>th</sup> August 2016  $M_w$  6.0 earthquake is also shown (red pointer).

after the mainshock were carried out for inventorying the earthquake-triggered ground effects, which resulted to be 147. The large part consists in landslides which affected mainly road cuts (i.e. 73%). The direct field surveying was integrated with remote sensing analyses, such as the interpretation of interferometric and optical images, to fill gaps due to the strongly limited accessibility both in case of high-mountain areas and in case of zones close to villages where the access was restricted.

Based on statistical and spatial distribution analyses performed in this paper, it seems not possible to single out a main local controlling factor in the spatial distribution of the inventoried effects, since a homogeneous abundance of involved lithologies can be observed, as well as a non-correlated distribution of effects with elevation and local MCS intensity. On the other hand, it is possible to output a decreasing frequency of effects with increasing epicentral distance, even if such a distribution does not indicate a so regular decay but a threshold close to 20 km from the epicentral areas. As it results from spatial analyses, the azimuthal distribution of the inventoried effect is strongly affected by man-made cut alignments such as roads and paths.

The distribution of ground effects triggered by the 24<sup>th</sup> August 2016 earthquake is clearly complementary to the ones obtained for the previous strong motions which struck adjacent areas in the last decades, i.e. the 1997 Umbria Marche and 2009 L'Aquila earthquakes, so filling the historical gap of the knowhow about such kind of earthquake-induced effects in Central Apennines.

## REFERENCES

- ALFARO P., DELGADO J., GARCIA-TORTOSA F.J., GINER J.J., LENTI L., LOPEZ-CASADO C., MARTINO S. & SCARASCIA MUGNOZZA G. (2012a) - *The role of near-field interaction between seismic waves and slope on the triggering of a rockslide at Lorca (SE Spain)*. Natural Hazards and Earth System Sciences, 12, 3631-3643.
- ALFARO P., DELGADO J., GARCIA-TORTOSA F.J., LENTI L., LOPEZ, J.A., LOPEZ-CASADO C. & MARTINO S. (2012b) - *Widespread landslides induced by the Mw 5.1 earthquake of 11 May 2011 in Lorca, SE Spain*. Engineering Geology, 137-138, 40-52.
- ARGNANI A. & RICCI LUCCHI F. (2001) - *Tertiary siliciclastic turbidite systems of the Northern Apennines*. In: VAI G.B. & MARTINI I.P. (Eds.) *Anatomy of an Orogen: The Apennines and Adjacent Mediterranean Basins*, 327-350.
- ARINGOLI D., CAVITOLLO P., FARABOLLINI P., GALINDO-ZALDIVAR J., GENTILI B., GIANO S.I., LÓPEZ-GARRIDO A.C., MATERAZZI M., NIBBI L., PEDRERA A., PAMBIANCHI G., RUANO P., RUIZ-CONSTAN A., SANZ DE GALDEANO C., SAVELLI D., TONDI E. & TROIANI F. (2014) - *Morpho-tectonic characterization of the quaternary intermontane basins of the Umbria-Marche Apennines (Italy)*. Rendiconti Lincei, 25/2, 11-128.
- ASHFORD S.A. & SITAR N. (1997) - *Analysis of topographic amplification of inclined shear waves in a steep coastal bluff*. Bulletin of Seismological Society of America, 87, 692-700.
- BALLY A.W., BURBI L., COOPER C. & GHELARDONI R. (1986) - *Balanced sections and seismic reflection profiles across the Central Apennines*. Memorie della Società Geologica Italiana, 35, 257-310.
- BIGI S., CENTAMORE E. & NISIO S. (1997) - *Elementi di tettonica quaternaria nella fascia pedeappenninica marchigiano-abruzzese*. Italian Journal of Quaternary Sciences, 10, 359-362.
- BIGI S. & COSTA PISANI P. (2005) - *From a deformed Peri-Tethyan carbonate platform to a fold-and-thrust-belt: an example from the Central Apennines (Italy)*. Journal of Structural Geology, 27, 523-539.
- BIGI S., CASERO P. & CIOTOLI G. (2011) - *Seismic interpretation of the Laga Basin; constraints on the structural setting and kinematics of the Central Apennines*. Journal of the Geological Society, 168, 179-190.
- BIRD J.F. & BOMMER J.J. (2004) - *Earthquake losses due to ground failure*. Engineering Geology, 75, 147-179.
- BONCIO P., LAVECCHIA G. & PACE B. (2004a) - *Defining a model of 3D seismic sources for Seismic Hazard Assessment applications: The case of central Apennines (Italy)*. Journal of Seismology, 8, 407-425.
- BONCIO P., LAVECCHIA G., MILANA G. & ROZZI B. (2004b) - *Seismogenesis in Central Apennines, Italy: an integrated analysis of minor earthquake sequences and structural data in the Amatrice-Campotosto area*. Annals of Geophysics, 47, 1723-1742.
- BONINI L., MAESANO F.E., BASILI R., BURRATO P., CARAFA M.M.C., FRACASSI U., KASTELIC V., TARABUSI G., TIBERTI M.M., VANNOLI P. & VALENSISE G. (2016) - *Imaging the tectonic framework of the 24 August 2016, Amatrice (central Italy) earthquake sequence: new roles for old players?* Annals of Geophysics, 59. doi: 10.4401/ag-7229.
- BOZZANO F., LENTI L., MARTINO S., MONTAGNA A. & PACIELLO A. (2011a) - *Earthquake triggering of landslides in highly jointed rock masses: Reconstruction of the 1783 Scilla rock avalanche (Italy)*. Geomorphology, 129, 294-308.
- BOZZANO F., LENTI L., MARTINO S., PACIELLO A. & SCARASCIA MUGNOZZA G. (2011b) - *Evidences of landslide earthquake triggering due to self-excitation process*. International Journal of Earth Sciences, 100, 861-879.
- CACCIUNI A., CENTAMORE E., DI STEFANO R. & DRAMIS F. (1995) - *Evoluzione morfotettonica della conca di Amatrice*. Studi Geologici Camerti, Volume Speciale 1995/2, 95-100.
- CALAMITA F., PALTRINIERI W., PELOROSSO M., SCISCIANI V. & TAVARNELLI E. (2003) - *Inherited mesozoic architecture of the Adria continental palaeomargin in the Neogene central Apennines orogenic system, Italy*. Bollettino della Società Geologica Italiana, 122, 307-318.
- CAMASSI R. & STUCCHI M. (1997) - *NT4.1, un catalogo parametrico di terremoti di area italiana al di sopra della soglia del danno. A parametric catalogue of damaging earthquakes in the Italian area*. versione NT4.1.1 Luglio 1997. <http://emidius.mi.ingv.it/NT/CONSNT.html>
- CANTALAMESSA G., CENTAMORE E., CHIOCCINI U., MICARELLI A. & POTETTI M. (1982) - *Tectonic-sedimentary evolution of north-western part of the Laga basin during the Upper Miocene-Lower Pliocene (Central-Southern Marche)*. Memorie della Società Geologica Italiana, 24, 221-232.
- CENTAMORE E. & NISIO S. (2003) - *Effects of uplift and tilting in the Central-Northern Apennines (Italy)*. Quaternary International, 101-102, 93-101.
- CIARAPICA G. & PASSERI L. (2002) - *The palaeogeographic duplicity of the Apennines*. Bollettino della Società Geologica Italiana, Special Volume, 1, 67-75.
- CIPOLLARI P. & COSENTINO D. (1991) - *La linea Olevano-Antradoco: contributo della biostratigrafia alla sua caratterizzazione cinematica*. Studi Geologici Camerti, Volume Speciale, 1991/2, 143-149.
- COLLINS B.D. & JIBSON R.W. (2015) - *Assessment of existing and potential landslide hazards resulting from the April 25, 2015 Gorkha, Nepal earthquake sequence (ver. 1.1, August 2015)*. U.S. Geological Survey Open-File Report 2015-1142, 50 pp., doi: 10.3133/ofr20151142.
- CPTI Working Group (2004) - *Catalogo Parametrico dei Terremoti Italiani, versione 2004 (CPTI04)*. INGV, Bologna, <http://emidius.mi.ingv.it>
- DELGADO J., GARRIDO J., LÓPEZ-CASADO C., MARTINO S. & PELÁEZ J. A. (2011) - *On far field occurrence of seismically induced landslides*. Engineering Geology, 123, 204-213.

- DEMANGEOT J. (1965) - *Geomorphologie des Abruzzes Adriatiques*. Mem. et Doc. Du C.N.R.S, Paris, 403 pp.
- DISS WORKING GROUP (2010) - *Database of Individual Seismogenic Sources (DISS), Version 3.1.1: A compilation of potential sources for earthquakes larger than M 5.5 in Italy and surrounding areas*. <http://diss.rm.ingv.it/diss/>
- DUSSAUGE C., GRASSO J.R. & HELMSTETTER A. (2003) - *Statistical analysis of rockfall volume distributions: Implications for rockfall dynamics*. Journal of Geophysical Research: Solid Earth, 108, 2286.
- EMERGEO WORKING GROUP (2016) - *Coseismic effects of the 2016 Amatrice seismic sequence: first geological results*. Annals of Geophysics, 59. doi: 10.4401/ag-7195.
- EVANS S. G. & BENT A. L. (2004) - *The Las Colinas landslide, Santa Tecla: A highly destructive flowslide triggered by the January 13, 2001, El Salvador earthquake*. GSA Special Papers, 375, 25-38.
- FALCINI F., MARINI M., MILLI S. & MOSCATELLI M. (2009) - *An inverse problem to infer paleoflow conditions from turbidites*. Journal of Geophysical Research, 114, C10019.
- FUBELLI G., DELLA SETA M. & AMATO G. (2014) - *Drainage system adjustment in response to the opening of the Rieti intermontane basin (Central Italy): geostatistical reconstruction of the PaleoFarfa River alluvial plain*. Rendiconti Lincei, Scienze Fisiche e Naturali, 25 (Suppl. 2), S167-S176. doi: 10.1007/s12210-014-0322-0
- FORTUNATO C., MARTINO S., PRESTININZI A., ROMEO R.W., FANTINI A. & SARANDREA A. (2012) - *New release of the Italian catalogue of earthquake-induced ground failures (CEDIT)*. Italian Journal of Engineering Geology and Environment, 2-5, 63-74.
- GALADINI F. & GALLI P. (2003) - *Paleoseismology of silent faults in the Central Apennines (Italy): the Mt. Vettore and Laga Mts. Faults*. Annals of Geophysics, 46, 815-836.
- GALLI P., PERONACE E., BRAMERINI F., CASTENETTO S., NASO G., CASONE F. & PALLONE F. (2016a) - *The MCS intensity distribution of the devastating 24 August 2016 earthquake in central Italy ( $M_W$  6.2)*. Annals of Geophysics, 59, Fast Track 5. doi: 10.4401/ag-7287.
- GALLI P., PERONACE E. & TERTULLIANI A. (2016b) - *Rapporto sugli effetti macrosismici del terremoto del 24 Agosto 2016 di Amatrice in scala MCS*. Roma, rapporto congiunto DPC, CNR-IGAG, INGV, 15 pp.
- GEER WORKING GROUP (2016) - *Engineering Reconnaissance of the 24 August 2016 Central Italy Earthquake. Version 2*. In: ZIMMARO P. & STEWART J.P. (Eds.) Report No. GEER-050B, doi: 10.18118/G61S3Z.
- GHISETTI F. & VEZZANI L. (1991) - *Thrust belt development in the central Apennines (Italy): Northward polarity of thrusting and out-of-sequence deformations in the Gran Sasso Chain*. Tectonics, 10, 904-919.
- GORUM T., FAN X.M., VAN WESTEN C.J., HUANG R.Q., XU Q., TANG C., & WANG G.H. (2011) - *Distribution pattern of earthquake-induced landslides triggered by the 12 May 2008 Wenchuan earthquake*. Geomorphology, 133(3-4), 152-167.
- GUZZETTI F., MALAMUD B.D., TURCOTTE D.L. & REICHENBACH P. (2002) - *Power-law correlations of landslide areas in central Italy*. Earth and Planetary Science Letters, 195, 169-183.
- HARP E. L., & JIBSON R. W. (1995) - *Inventory of landslides triggered by the 1994 Northridge, California earthquake*. U.S. Geological Survey Open-File Report 95-213.
- HARP E.L. & JIBSON R.W. (2002) - *Anomalous concentrations of seismically triggered rock falls in Pacoima Canyon: are they caused by highly susceptible slopes or local amplification of seismic shaking?* Bulletin of Seismological Society of America, 92, 3180-3189.
- HOVIUS N., STARK C.P. & ALLEN P.A. (1997) - *Sediment flux from a mountain belt derived by landslide mapping*. Geology, 25, 231-234.
- HUNGR O., EVANS S.G. & HAZZARD J. (1999) - *Magnitude and frequency of rock falls and rock slides along the main transportation corridors of southwestern British Columbia*. Canadian Geotechnical Journal, 36, 224-238.
- ISPRA (2016) - *Report attività svolta da ISPRA in data 25-26/08/2016, A (in Italian)*. Available at: <http://www.isprambiente.gov.it/files/notizie-ispra/notizie-2016/sisma-italiacentrale/ReportattivitsvoltadaISPRAindata26.pdf>, last accessed October 19, 2016.
- KEEFER D.K. (1984) - *Landslides caused by earthquakes*. Bulletin of the Geological Society of America, 95, 406-421.
- KEEFER D.K. (2000) - *Statistical analysis of an earthquake-induced landslide distribution in the 1989 Loma Prieta, California event*. Engineering Geology, 58, 231-249.
- KHAZAI B. & SITAR N. (2004) - *Evaluation of factors controlling earthquake-induced landslides caused by Chi-Chi earthquake and comparison with the Northridge and Loma Prieta events*. Engineering Geology, 71, 79-95.
- LANZANO G., LUZI L., PACOR F., PUGLIA R., D'AMICO M., FELICETTA C. & RUSSO E. (2016) - *Preliminary analysis of the accelerometric recordings of the August 24<sup>th</sup>, 2016  $M_W$  6.0 Amatrice earthquake*, Annals of Geophysics, 59, Fast Track 5. doi: 10.4401/ag-7201
- LOVATI S., BAKAVOLI M., MASSA M., FERRETTI G., PACOR F., PAOLUCCI R., HAGHSHENAS E. & KAMALIAN M. (2011) - *Estimation of topographical effects at Narni ridge (Central Italy): comparison between experimental results and numerical modelling*. Bulletin of Earthquake Engineering, 9, 1987-2005.
- MALAMUD B.D. & TURCOTTE D.L. (1999) - *Self-organized criticality applied to natural hazards*. Natural Hazards, 20, 93-116.
- MALAMUD B.D., TURCOTTE D.L., GUZZETTI F. & REICHENBACH P. (2004) - *Landslide inventories and their statistical properties*. Earth Surface Processes and Landforms, 29, 687-711.
- MARTHA T.R., ROY P., MAZUMDAR R., BABU GOVINDHARAJ K. & VINOD KUMAR K. (2017) - *Spatial characteristics of landslides triggered by the 2015  $M_w$  7.8 (Gorkha) and  $M_w$  7.3 (Dolakha) earthquakes in Nepal*. Landslides, 14 (2), 697-704. doi: 10.1007/s10346-016-0763-x
- MARTINO S., PRESTININZI A. & ROMEO R.W. (2014) - *Earthquake-induced ground failures in Italy from a reviewed database*. Natural Hazards and Earth System Sciences, 14, 799-814.
- MELETTI C., GALADINI F., VALENSISE G., STUCCHI M., BASILI R., BARBA S., VANNUCCI G. & BOSCHI E. (2008) - *A seismic source zone model for the seismic hazard assessment of the Italian territory*. Tectonophysics, 450, 85-108.
- MEUNIER P., HOVIUS N., & HAINES A.J. (2007) - *Regional patterns of earthquake-triggered landslides and their relation to ground motion*. Geophysical Research Letters, 34, L20408.
- MEUNIER P., HOVIUS N., & HAINES J.A. (2008) - *Topographic site effects and the location of earthquake induced landslides*. Earth and Planetary Science Letters, 275, 221-232.
- MICHETTI A.M., ESPOSITO E., GURPINAR A., MOHAMMADIOUN B., MOHAMMADIOUN J., PORFIDO S., ROGOZHIN E., SERVA L., TATEVOSSIAN R., VITTORI E., AUDEMARD F., COMERCI V., MARCO S., MCCALPIN J. & MORNER N.A. (2004) - *The INQUA Scale. An innovative approach for assessing earthquake intensities based on seismically induced ground effects in natural environment*. Memorie descrittive della Carta Geologica d'Italia, 67.
- MOORE J.R., GISCHIG V., BURJANEK J., LOEW S. & FAH D. (2011) - *Site effects in unstable rock slopes: dynamic behaviour of the Randa instability (Switzerland)*. Bulletin of Seismological Society of America, 101, 3110-3116.
- NISIO S. (1997) - *Evoluzione geologica e morfotettonica dell'area compresa tra il Gran Sasso ed il Mare Adriatico*. Geologica Romana, 33, 13-27.
- PAGE P., CALAMITA F. & TAVARNELLI E. (2015) - *Brittle-ductile shear zones along inversion-related frontal and oblique thrust ramps. Insights from*

- the Central-Northern Apennines curved thrust system (Italy)*. In: MUKHERJEE S. & MULCHRONE K.F. (Eds.) *Ductile Shear Zones: from micro- to macro-scales*, Wiley, 111-127.
- PAPADOPOULOS G. & PLESSA A. (2000) - *Magnitude-distance relations for earthquake-induced landslides in Greece*. *Engineering Geology*, 58, 377-386.
- PETLEY D.N. (2012) - *Global patterns of loss of life from landslides*. *Geology*, 40, 927-930.
- PIERANTONI P., DEIANA G. & GALDENZI S. (2013) - *Stratigraphic and structural features of the Sibillini Mountains (Umbria-Marche Apennines, Italy)*. *Italian Journal of Geosciences*, 132, 497-520.
- PIZZI A. & GALADINI F. (2009) - *Pre-existing cross-structures and active fault segmentation in the northern-central Apennines (Italy)*. *Tectonophysics*, 476, 304-319.
- RICCI LUCCHI F. (1986) - *The Oligocene to recent foreland basins of the Northern Apennines*. In: ALLEN P.A. & HOMEWOOD P. (Eds.) *Foreland basins*, Blackwell Publishing Ltd., Oxford, UK, 103-139.
- RODRIGUEZ C. E., BOMMER J. J. & CHANDLER, R. J. (1999) - *Earthquake-induced landslides: 1980-1997*. *Soil Dynamics and Earthquake*, 18, 325-346.
- SABETTA F. & PUGLIESE A., (1987) - *Attenuation of peak horizontal acceleration and velocity from Italian strong-motion records*. *Bulletin of the Seismological Society of America*, 77, 491-1513.
- STARK C.P. & GUZZETTI F. (2009) - *Landslide rupture and the probability distribution of mobilized debris volumes*. *Journal of Geophysical Research: Earth Surface*, 114, F00A02.
- STARK C.P. & HOVIUS N. (2001) - *The characterization of landslide distributions*. *Geophysical Research Letters*, 28, 1091-1094.
- STUCCHI M., CAMASSI R., ROVIDA A., LOCATI M., ERCOLANI E., MELETTI C., MIGLIAVACCA P., BERNARDINI F. & AZZARO R. (2007) - *DBMI04, il database delle osservazioni macrosismiche dei terremoti italiani utilizzate per la compilazione del catalogo parametrico CPTI04*. *Quaderni di Geofisica*, 49, 38 pp. <http://emidius.mi.ingv.it/DBMI04>
- TATARD L., GRASSO J. R., HELMSTETTER A. & GARAMBOIS S. (2010) - *Characterization and comparison of landslide triggering in different tectonic and climatic settings*. *Journal of Geophysical Research: Earth Surface*, 115(F4).
- TONDI E. & CELLO G. (2003) - *Spatio-temporal evolution of the central Apennines fault system (Italy)*. *Journal of Geodynamics*, 36, 113-128.
- VALAGUSSA A. & FRATTINI P. (2016) - *Relationship between earthquake-induced landslides magnitude, ground motion and distance from the seismic source*. *Rendiconti della Società Geologica Italiana*, 41, 350-353.
- VARNES D.J. (1978) - *Slope movement types and processes*. In: SCHUSTER R.L. & KRIZEK R.J. (Eds.) *Special Report 176: Landslides: Analysis and control*. Transportation and Road research board, National Academy of Science, Washington D.C., 11-33.
- WARTMAN J., DUNHAM L., TIWARI B. & PRADEL D. (2013) - *Regional patterns of landslides from the 2011 Tohoku Japan earthquake*. In: LOLLINO G. & alii (Eds.) *Engineering Geology for Society and Territory - Volume 2: Landslide Processes*, 758-764. doi: 10.1007/978-3-319-09057-3\_128.
- XU C., XU X. YAO X., & DAI F. (2014) - *Three (nearly) complete inventories of landslides triggered by the May 12, 2008 Wenchuan Mw 7.9 earthquake of China and their spatial distribution statistical analysis*. *Landslides*, 11 (3), 441-461.
- ZEVENBERGEN L.W. & THORNE C.R. (1987) - *Quantitative analysis of land surface topography*. *Earth Surface Processes and Landforms*, 12, 47-56.

(Ms. received 2 March 2017; accepted 29 May 2017)

